Accepted Manuscript

Journal of the Geological Society

Spatial variation in provenance signal: identifying complex sand sourcing within a Carboniferous basin using multiproxy provenance analysis.

B. Anders, S. Tyrrell, D. Chew, C. Mark, G. O'Sullivan, J. Murray, J.R. Graham & E. Badenszki

DOI: https://doi.org/10.1144/jgs2021-045

To access the most recent version of this article, please click the DOI URL in the line above. When citing this article please include the above DOI.

Received 10 April 2021
Revised 14 July 2021
Accepted 28 July 2021

Supplementary material at https://doi.org/10.6084/m9.figshare.c.5536691

nSpatial variation in provenance signal: identifying complex sand sourcing within a Carboniferous basin using multiproxy provenance analysis.

B. Anders[1,2], S. Tyrrell [1,2,3], D. Chew[4,3], C. Mark[5], G. O'Sullivan[5], J. Murray[1,3], J.R. Graham[4], E. Badenszki[3,5]
Corresponding author: (b.anders1@nuigalway.ie)
[1] *Earth and Ocean Sciences, School of Natural Sciences, NUI Galway, University Road, Galway.*
[2] *Sediment Origins Research Team (SORT), NUI Galway, Ireland.*
[3] *Irish Centre for Research in Applied Geosciences (iCRAG).*
[4] *Department of Geology, Trinity College Dublin, College Green, Dublin 2.*
[5] *UCD School of Earth Sciences, University College Dublin, Belfield, Dublin 4.*

Abstract: Multiple factors (e.g. source rock composition, climate, nature/scale of sedimentary system) influence the volume and composition of sediment delivered to basins. Fluctuations in these parameters produce cryptic source signals which can vary within the same sedimentary system. Bespoke multi-proxy provenance approaches, targeted at minerals of variable stability, allow for an assessment of natural biasing (recycling) and intra-basinal spatial variations.

Provenance of fluvial/deltaic sandstones (Mullaghmore Sandstone Formation) in the NW Carboniferous Basin, Ireland, has been constrained using zircon and apatite U-Pb geochronology, trace elements in apatite and Pb-in-K-feldspar analysis. Zircon U-Pb grain populations are consistent with feldspar data, suggesting Proterozoic basement highs offshore Ireland and Scotland were the main contributor with minor supply from Archean-Palaeoproterozoic rocks of Greenland/NW Scotland and Caledonian-aged rocks. However, apatite data shows a much larger proportion of Caledonian-aged grains of metamorphic origin, suggesting significant sediment was recycled from Neopropterozoic metasedimentary rocks. The spatial variation in provenance indicates that, at onset of clastic input, sediment was being routed to the basin through a complex drainage system, comprising of several discrete hinterland catchments, rather than supply from a single, large interconnected sedimentary system. Such complexities can only be identified with the careful application of a bespoke multi-proxy provenance approach.

Sedimentary provenance analysis refers to the study of sediment origin and encompasses all of the factors related to the production of clastic sediment or sedimentary rocks (Pettijohn *et al.*, 2012). This not only involves the identification of the original sediment source, but also determining the transport mechanisms and pathways that delivered sediment to a depositional basin. Provenance has many applications; it is widely used in "source to sink" studies (Tinker *et al.*, 2008; Blowick *et al.*, 2019), in understanding the nature and distribution of potential hydrocarbon reservoirs (Rossi *et al.*, 2002) and in correlating stratigraphic units (Kalsbeek *et al.*, 2008; Morton *et al.*, 2011; Hurst and Morton, 2014). It is also used in reconstructing palaeogeography and constraining deep time continental plate movement (Dickinson, 1988), in assessing ice-sheet movement/dynamics through sourcing ice-rafted debris (Hemming *et al.*, 1996; Flowerdew *et al.*, 2013; Flowerdew *et al.*, 2019) and in palaeoclimate studies (Ding *et al.*, 2001; Yan *et al.*, 2007; Meyer *et al.*, 2011)

Basic sedimentological (e.g. sedimentary structures, paleoflow indicators and lithofacies) and petrological (e.g. rock composition and texture) information has long been used in provenance studies as a primary indicator of likely source lithology and transport direction (e.g. Sorby, 1880). This primary data is useful to contextualise more detailed geochemical provenance information. With the recent advent of sophisticated, widely available and relatively inexpensive analytical facilities, the application of geochemical and isotopic techniques to investigate whole-rock or individual sediment grains has increased dramatically (Gard *et al.*, 2019). Laser ablation inductively coupled plasma mass spectrometry (LA-ICP-MS) has now largely supplanted secondary ion mass spectrometry (SIMS) and sensitive high resolution ion microprobe (SHRIMP) techniques in sedimentary provenance studies, permitting rapid acquisition of data (Machado and Gauthier, 1996; Chew *et al.*, 2019a) that is unparalleled by other methods. Mineral chemistry and composition (including elemental concentrations, isotope ratio tracers and geochronological data) can be assessed from a range of detrital grains, yielding useful provenance information. However, as has been noted by recent researchers (Flowerdew *et al.*, 2019; Franklin *et al.*, 2019; Mulder *et al.*, 2019; Guo *et al.*, 2020; Nauton-Fourteu *et al.*, 2020; Deng *et al.*, 2021), the use of a single provenance

proxy, in isolation and focussed on only one unique mineral phase, can result in misinterpretation of the provenance signal due to contrasting behaviour of different minerals during transport and burial (Morton and Hallsworth, 1999; Ibañez-Mejia *et al.*, 2018; Chew *et al.*, 2020), relative abundance of minerals in bedrock sources (Moecher and Samson, 2006; Dickinson, 2008; Flowerdew *et al.*, 2019) and sediment recycling (Dickinson *et al.*, 2009; Tyrrell *et al.*, 2009; Barham *et al.*, 2020). Multi-proxy approaches have been utilised more frequently in recent years (Flowerdew *et al.*, 2019; Franklin *et al.*, 2019; Mulder *et al.*, 2019; Blowick *et al.*, 2020a; Nauton-Fourteu *et al.*, 2020) in order to address these issues.

It is well established that the provenance signal in a sediment or sedimentary rock is a function of source rock composition, climate, transport, depositional environment, diagenesis, burial and weathering (von Eynatten and Dunkl, 2012). Other, less well understood factors influencing provenance signal include very broadly the scale and dynamics of a sedimentary system and at a more local scale mixing (by discharge, currents, waves, differential settling etc.). Both of these factors are interrelated, and sediment residence time, which is a function of transport mechanism, distance, energy and scale, should ultimately control the extent to which sediment (and consequently the provenance signal) is fractionated, mixed and achieves homogeneity in any given basin with respect to its sources.

It is reasonable to assume that bedload sediment deposited within a fluvial channel should display a provenance signal of the hinterland sourced exclusively by that river system. Conversely, sediment deposited on a shelf, away from direct points of input, is likely to represent a mix of sources entering onto that shelf. This implies that unless a sedimentary system is extremely well mixed and homogenised, the provenance signal should be retained, but will vary within a basin depending on depositional environments and facies (Garzanti and Andò, 2007). Furthermore, basin geometry and the number of unique input points may lead to spatial variation of provenance signal throughout a basin.

This paper aims to provide more clarity on the more cryptic factors controlling variation in provenance signal by assessing the sourcing of sedimentary sequences in the North West Carboniferous Basin (NWCB), a relatively modest-scale basin onshore west of Ireland. The focus of this study is the mid-Viséan Mullaghmore Sandstone Formation (MSFm), a clastic unit enclosed in a largely carbonate-dominant sequence (Figs. 1,2). It is an ideal testing site as there is excellent exposure at multiple locations on the NW coast of Ireland, with abundant medium – coarse grained channel sandstones. The MSFm comprises a range of sedimentary facies, with facies packages representing several depositional settings including continental shelf shallow shore-face, deltaic channels and terrestrial fluvial palaeoenvironments. In order to assess spatial variation in provenance signal and remove complexity introduced by shelf mixing (Fig. 3), this study concentrates on channel sandstone facies developed in the MSFm, with a focus on the basal (lowermost) channels. This approach aims to capture information on the initial sediment influx to the basin, and targeting of the channel sandstones should provide the most accurate representation of the source terranes drained by the fluvial system responsible for supplying clastic sediment to the NWCB, prior to mixing on the paleo-shelf. Additionally, the targeting of several, broadly time-equivalent, basal channel sandstones over the area of the NWCB permits an assessment of spatial variation in provenance signal. This approach will help constrain the nature, scale and dynamics of the supply system (e.g. identifying a large interconnected drainage system versus multiple smaller rivers).

As well as standard optical microscopy, a multi-proxy provenance approach is used (zircon and apatite U-Pb geochronology, trace elements in apatite and Pb-in-K-feldspar) to investigate a range of detrital minerals with known differing behaviours in sedimentary systems. Using all these proxies maximises insight into the fluctuating sand supply to the NWCB as well as clarifying, more generally, the potential contrasting information stored in provenance proxies based on minerals with variable behaviour in the sedimentary environment.

The North West Carboniferous Basin, Ireland

Geological context and setting

During the early Carboniferous (lower Mississippian) north-western Europe was dominated by widespread carbonate production and local drainage systems. Later, during the upper Mississippian and Pennsylvanian, medium- to large-scale river systems developed, largely derived from uplands associated with the Caledonian or nascent Variscan orogenic belts (Leeder, 1988), and siliciclastic sedimentation (in fluvial, deltaic, shallow- and deep-marine settings) became more prevalent. The progressive onset of the Late Paleozoic Ice Age during the Mississippian (Davies and Fielding, 2008; Fielding *et al.*, 2008) is associated with dynamic oscillations in paleoclimate, with an overall trend towards more arid conditions. Continued diversification of terrestrial vegetation provided stability and encouraged more mature soil development (Davies and Gibling, 2013). These varied factors led, for example, to the development of the Pennine drainage system in Britain (Leeder, 1988) and smaller scale Shannon Basin system in Ireland (Pulham, 1989), with associated deltaic deposits.

Ireland was positioned in tropical latitudes just south of the palaeoequator during the Mississippian (Blakey, 2008). Following a regional northwards transgression during the Tournaisian (Graham and Sevastopulo, 2020), marine carbonate sedimentation became prevalent and continued through the Viséan, with deposition occurring across a series of shallow platforms and intervening intracratonic basins (Leeder, 1982, 1987; Sevastopulo and Wyse Jackson, 2009). The NWCB was one of these basins and it was infilled initially by basal clastics deposited unconformably on Dalradian basement, before becoming carbonate-dominated (typically limestone and shale lithologies; (Philcox *et al.*, 1992; Somerville *et al.*, 2009; Barham *et al.*, 2012). A regional lowstand event during the mid-Viséan is interpreted as the cause of a distinct clastic input event represented by the MSFm. This unit is dated as late Arundian to Holkierian based on miospore (Higgs, 1984; Clayton, 1985) and foraminiferal (Graham, 1996) evidence. Clastic units of a similar age are not a conspicuous feature of Viséan successions elsewhere in Ireland, most likely due to the particular palaeogeographic and

depositional configuration of the NWCB: terrestrial palaeoenvironments were located immediately to the north and northwest (Scotese and McKerrow, 1990) and much of the area around Donegal Bay (Fig. 1) is believed to have been located close to the coastal zone (Graham, 1996, 2017).

The base of the MSFm is interpreted as a sequence boundary, produced by an estimated drop in sea-level of 8m (Graham, 1996). The base of the formation is typically erosive, with over 4m of relief noted in a cliff section at the most fluvially-influenced location at Creevagh Head in North Mayo (Fig. 2a). While dominantly marginal marine in nature, depositional environments and erosional character vary within the MSFm. The underlying early Viséan Moyny Limestone Formation in north Mayo is interpreted as representing fully marine conditions (Sevastopulo & Wyse Jackson 2009), with channel sandstones in the upper part of the unit in north Mayo representing tidal channels (Graham, 1996). By contrast, the MSFm is interpreted as representing a more fluvio-deltaic environment. Sub-environments include interdistributary bay (Kilcummin, location 2), lateral delta lobe (Carrowmoran, location 3) and proximal-to-landmass deltaic environments (Bundoran and Mullaghmore Head locations 4a & 4b); see Figs. 1, 2 & 4 for locations and stratigraphic correlation.

The Tournaisian marine transgression coincided with a phase of (broadly N-S) crustal extension, which led to basin development in Ireland and Britain (Worthington and Walsh, 2011). The initial main phase of rifting occurred during the Tournaisian to early Viséan and was followed by a phase of tectonic quiescence and slow subsidence later in the Viséan (between the Arundian and early Asbian regional substages), during which the MSFm was deposited. Renewed tectonic activity occurred in Britain and Ireland in the late Viséan and Serpukhovian (e.g. Philcox *et al.*, 1992; Kelly, 1996); however, the Carboniferous succession of the NWCB experienced minimal post depositional deformation (Graham, 2010).

Graham (1996) noted that whilst a detailed understanding of provenance for the MSFm remained to be ascertained, sediment had evidently been derived from the NNW. Philcox et al. (1992) noted that the MSFm thinned and grain size reduced in a southerly direction within the Lough Allen sub-basin.

The feldspathic nature of the sandstones and presence of strained quartz (Oswald, 1955; Graham, 1996; MacDermot, 1996; Connolly, 2003; Graham, 2010, 2017) in the MSFm suggests a source comprising mixed igneous (likely felsic) and metamorphic rocks (likely the Dalradian Supergroup, discussed below); however, more sophisticated single grain provenance techniques have not been previously applied.

Potential source terranes for the Mullaghmore Sandstone Fm

Based on the current onshore and offshore sub-sea geology, potential source areas to the north and northwest of the NCWB likely comprised a complex array of Archean and Proterozoic terranes which amalgamated during the Caledonian Orogenic Cycle. These areas are associated with the Laurentian continent, a large landmass which comprised of the North American and Greenland continents, and also included northwest Ireland and Scotland (Chew and Strachan, 2014). This landmass contained components of Archean crust, such as in the Lewisian Complex and the Nagssugtoqidian. The basement source terrane map (Fig. 5; Table 1) illustrates the relative locations and age of upland terranes during the Carboniferous.

The central region of the Lewisian Complex contains c. 2.7 – 2.9 Ga gneisses associated with the Scourian metamorphic event which later experienced Laxfordian magmatism and metamorphism (c. 1.8 – 1.6 Ga) during the Paleoproterozoic (Whitehouse and Moorbath, 1986; Kinny *et al.*, 2005). The Stanton Banks (offshore northwest Scotland) is Paleoproterozoic in age and interpreted to be surrounded by Archean rocks (Scanlon *et al.*, 2003).

Southern Greenland is comprised of three major and broadly E-W striking geological belts which from south to north are (Fig. 5; table 1)

1) the Paleoproterozoic (Statherian) Ketilidian Belt (Garde *et al.*, 2011);

2) the Archean North Atlantic Craton (NAC; also known as Archean Craton; (Nutman and Friend, 2007; Strachan *et al.*, 2020); and

3) Meso- to Neoarchean orthogneisses of the Nagssugtoqidian, which were reworked during the Paleoproterozoic (1.85-1.75 Ga; (Connelly and Thrane, 2005; Johnston and Kylander-Clark, 2013).

It has been suggested that the Nagssugtoqidian and Lewisian Complex terranes are potential correlatives (Kalsbeek *et al.*, 1993; Chadwick and Garde, 1996; Daly, 1996; Tyrrell *et al.*, 2009), as they appear to have experienced similar orogenic histories and yield similarly aged rocks – thus implying that their detrital signals potentially cannot be distinguished. However, the Nagssugtoqidian has subtly different K-feldspar Pb isotopic signatures to the Lewisian Complex, rendering them distinguishable by that method (Tyrrell *et al.*, 2009).

A number of modern bathymetric highs, offshore Ireland and UK (Fig. 5; table 1) are known to comprise elements of Paleoproterozoic to Mesoproterozoic crust. These are likely stranded remnants of crustal blocks of Laurentian-affinity that were isolated after the Atlantic Ocean opened. These may have had more significant topographic expression in the past. These highs include the Porcupine High, Hebridean Plateau, Rockall Bank and Hatton Bank. Given the difficulty with direct sampling of submarine outcrops, these have been constrained in just few locations and often by indirect sampling methods (e.g. sea floor dredging). However, the available data appears to show that these highs are of broadly similar composition , affinity and age (Morton *et al.*, 2009), and known to contain Paleoproterozoic to Mesoproterozoic crust. These highs also appear to have experienced several regionally significant orogenic events including the Labradorian at 1.71-1.62 Ga (Morton and Taylor, 1991), Pinwarian between 1.51 – 1.45 Ga (McAteer *et al.*, 2010) and Grenvillian event between 1.3-0.9 Ga (McLelland *et al.*, 1996; Chew *et al.*, 2019b).

Onshore west Ireland, the Annagh Gneiss Complex (AGC) comprises highly deformed orthogneisses ranging from Paleoproterozoic to Neoproterozoic in age (Fig. 5; table 1). This terrane experienced Grenvillian deformation between 1.18 Ga and 0.96 Ga (Daly, 1996). The Rhinns Complex (RC) is found on Inishtrahull, the Isle of Colonsay and in the Hebrides and represents Paleoproterozoic

basement (1.9 – 1.7 Ga) (Muir *et al.*, 1992) composed of mainly syenite and gabbro with minor felsic and mafic intrusions. However, unlike the AGC, the RC has not experienced Grenville deformation. Both the AGC and RC are thought to comprise the geological basement onshore north Ireland and Scotland respectively (Daly, 1996; Cawood *et al.*, 2003; Flowerdew *et al.*, 2009).

Neoproterozoic metasedimentary rocks of the Dalradian Supergroup structurally overlie the AGC in northwest Ireland (Cawood *et al.*, 2003; Stephenson *et al.*, 2013) and were originally deposited on the southern Laurentian margin and ultimately sourced from the Laurentian continent. These metasedimentary rocks are potentially a significant source for polycyclic heavy mineral grains (possibly both zircon and apatite) (Cawood *et al.*, 2003; Henrichs *et al.*, 2018).

Igneous activity associated with the Caledonian Orogenic Cycle (the closure of the Iapetus Ocean and collision of Laurentia, Avalonia and Baltica) resulted in the regional emplacement of various granitic bodies during the Ordovician to Devonian (Stephenson *et al.*, 2013), including the volumetrically large plutons of the Donegal Granite ranging in age from 431-416 Ma (Archibald *et al.*, 2021) and more minor granitic intrusions in NW Ireland (Ox Mountain Granodiorite (Chew and Schaltegger, 2005). Such intrusions likely occur subsurface in the offshore areas along the Great Glen Fault (GGF; see Fig. 5) (Strachan *et al.*, 2020). Ultramafic lamprophyre dykes and appinite intrusion are also common within the northern part of the Caledonian Belt in Britain and Ireland (Morrison *et al.*, 2011) with mid-Silurian - Devonian ages recorded in such rocks in Donegal (Murphy, 2019; Archibald *et al.*, 2021) The Caledonian Orogenic Cycle has been divided into the Grampian (475–465 Ma and associated with regional greenschist to amphibolite facies-grade metamorphism of the Dalradian Supergroup); Scandian (435–425 Ma; restricted to northern Scotland, Norway and Eastern Greenland (Strachan *et al.*, 2020); and Acadian (405-390 Ma; recorded in Ireland only by upper-crustal brittle deformation and magmatism:(Chew and Stillman, 2009) orogenies.

Methodology

Outcrop and petrographic investigation of the Mullaghmore Sandstone Fm

Five key sections of the MSFm were examined and logged in the northwest of Ireland (Fig. 1, 2 & 3; Table 2) and facies associations determined. Throughout this paper, for simplicity, sample 1 refers to location 1; sample 2 refers to location 2 etc. For this study the basal channel sandstones in the MSFm were targeted (i.e. the first thick channel sandstone in the succession at Bunatrahir West and Bundoran (locations 1,4a respectively). A topmost channel sandstone at Mullaghmore Head and a near-to-top channel sandstone at Carrowmoran and Kilcummin (locations 4b and 3, 2 respectively) were also sampled. Location 4b was positioned stratigraphically ~100m above the first channel sandstone at location 4a) in the MSFm.

Thin sections were prepared from hand-samples recovered at outcrop, and polished to 30µm for conventional petrographic analysis using optical microscopy. Point counting and modal analysis was completed at NUIG with an optical polarising microscope and the PetrogLite software.

Pb-in-K-feldspar analysis

In preparation for Pb-in-K-feldspar analysis, 300 µm thick sections were prepared. These were first imaged with a Hitachi TM-1000 Desktop Scanning electron microscope (SEM) at NCIG (National Centre for Isotope Geochemistry) in UCD. This process helps identify any heterogeneties within grains, which can then be avoided during laser ablation. In-situ Pb isotopic composition of K-feldspars was analysed with a ThermoScientific Neptune MC-ICPMS at the National Centre for Isotope Geochemistry (NCIG) at University College Dublin. For sample 3, the Neptune MC-ICPMS was coupled with a NewWave 193 nm excimer laser while a Teledyne Cetac Analyte G2 193 nm excimer laser system was used for all other samples. The New Wave laser was operated using a variable fluence ranging from 4.9 to 6.5 $mJcm^{-2}$, a 20 Hz repetition rate with a 100 µm spot size. The Teledyne Cetac laser parameters were 4 $mJcm^{-2}$ fluence and 20 Hz repetition rate with a variable

spot size for unknowns ranging from 30 to 100 µm, depending on the size of the analysed K-feldspar grain.

For the Neptune MC-ICPMS an all-Faraday cup detector configuration was used and analytical approach closely followed the procedure described by (Tyrrell *et al.*, 2012). Isotopes ^{204}Pb, ^{206}Pb, ^{207}Pb and ^{208}Pb were measured simultaneously with ^{202}Hg, in order to correct for isobaric interference of ^{204}Hg on ^{204}Pb. ^{203}Tl and ^{205}Tl were also measured and employed during standard-sample bracketing to correct for instrumental bias. An in-house Excel spreadsheet was used to calculate the ^{208}Pb/^{204}Pb, ^{207}Pb/^{204}Pb and ^{206}Pb/^{204}Pb lead isotopic ratios. For data interpretation, we graphically report ^{207}Pb/^{204}Pb and ^{206}Pb/^{204}Pb ratios (Fig. 7); full isotope ratio data are reported in the Supplementary Information. During analysis the average ^{208}Pb signal for an 88 µm spot size ranged from 0.1 V – 2 V. Analysed grains with uncertainties > 0.5 % (2σ) were not included.

NIST612 was used as primary standard analysed after every 3 unknowns. Shap K-feldspar was analysed periodically as a secondary standard (Souders and Sylvester, 2010) in order to monitor data reduction. Shap feldspar has a well characterised Pb isotopic compostion (^{206}Pb/^{204}Pb) = 18.286. Previous work (Blowick *et al.*, 2020b) has suggested that a minimum of 40 K-feldspar grains are required for a 95% confidence that all contributing sources will be identified , hence this number was targeted (though not always achieved) in each sample.

Apatite and zircon analysis

For heavy mineral separation, whole rock samples were crushed using a jaw crusher and subsequently sieved into a 63 - 125µm size fraction. Standard procedure heavy mineral separation was carried out using LPT (lithium polytungstate) which has a density of 2.85 g/mL. The heavy mineral fraction was then magnetically separated, from which zircon and apatite grains were hand-picked from the non-magnetic fraction. In order to reduce selection bias while picking, small grids were drawn onto the base of the petri-dish and every zircon and apatite grain was picked per grid square, regardless of size or appearance, until no further grains could be identified in that grid square, or 150 grains in total were picked. Grains were mounted in epoxy resin and polished to

expose the centre of the grain. CL imaging was conducted for zircon grains and the grain centre was targeted during analysis. Analysis was carried out at the iCRAGLabs@TCD (Trinity College Dublin) using an Agilent 7900 Q-IC-PMS coupled with a Photon Machines Analyse Excite 193 nm ArF Excimer laser with a Helix 2 volume ablation cell. The laser was operated at 2.31 J/cm^2 with a repetition rate of 11 Hz. Spot sizes were 24 µm for zircon and 60 µm for apatite. Isotopes measured during zircon and apatite geochronology were $^{207}Pb/^{206}Pb$, $^{206}Pb/^{238}U$ and $^{207}Pb/^{235}U$.

The primary standards used for zircon and apatite were 91500 zircon and Madagascar apatite respectively (Wiedenbeck *et al.*, 1995; Thomson *et al.*, 2012). The secondary reference materials used were WRS-1348 and Plešovice zircon (Sláma *et al.*, 2008; Pointon *et al.*, 2012); as well as McClure Mountain and Durango apatite (McDowell *et al.*, 2005; Schoene and Bowring, 2006). Primary standards and secondary reference materials were analysed in blocks after ever ~30 unknowns. Trace elements in apatite were acquired simultaneously along with the U-Pb isotope data. Trace elements measured were: ^{55}Mn, ^{88}Sr, ^{89}Y, ^{90}Zr, ^{139}La, ^{140}Ce, ^{141}Pr, ^{146}Nd, ^{147}Sm, ^{153}Eu, ^{157}Gd, ^{159}Tb, ^{163}Dy, ^{165}Ho, ^{166}Er, ^{169}Tm, ^{172}Yb, ^{175}Lu, ^{232}Th and ^{238}U. Trace element data reduction employed NIST612 as the primary standard and a well characterised aliquot of Durango apatite as the secondary reference (Chew *et al.*, 2016).

Data reduction was undertaken using the Iolite plugin for the Igor Pro software (Paton *et al.*, 2011). U-Pb zircon data were reduced using the VizualAge Data Reduction Scheme (DRS) (Petrus and Kamber, 2012) and apatite data using the VizualAge UcomPbine DRS (Chew *et al.*, 2014) which accounts for variable common Pb in the primary apatite standard material. A downhole fractionation correction is calculated from the primary standard, which is then applied to all unknowns, as are corrections for fractionation, mass bias and instrument drift during the session.

Only concordant zircon analyses were employed, using a probability of concordance threshold of >0.001 as determined by the Concordia Age formula of Isoplot v4.15, (Ludwig, 2012). Apatite commonly contains significant amounts of common Pb along with relatively low U contents. Apatite

grains are thus commonly discordant, and the detrital apatite grains in this study were common Pb corrected using an iterative ^{207}Pb-based correction (Chew *et al.*, 2011) expanding from a starting estimate for $^{207}Pb/^{206}Pb$ initial ratio calculated using the terrestrial lead evolution model of (Stacey and Kramers, 1975). As apatite grains cannot be screened for discordance, an age uncertainty filter is instead applied as follows: >2 Ga 10% uncertainty, 2-1 Ga 15% uncertainty, 1-0.5 Ga 20% uncertainty and <500 Ma 25% uncertainty, following the approach of (Mark *et al.*, 2016). All concordias and Kernel Density Estimates (KDEs) were plotted in R. Previous studies have suggested that in order to achieve a 95% statistical probability in identifying all detrital populations 117 grains should be analysed in provenance studies based on geochronological studies (Vermeesch, 2004). This does not imply that studies with lesser grain counts do not still yield useful information for provenance interpretations.

Apatite trace elements were reduced using the Iolite Trace Element DRS, implementing the internal elemental standardisation approach of (Woodhead *et al.*, 2007). Trace element data were plotted using the approach described by (O'Sullivan *et al.*, 2020), which feeds a reference dataset of published apatite trace element compositions from c. 360 bedrock samples to a machine learning classifier algorithm (support vector machine) in order to provide an estimate of likely lithology for unknown (i.e. detrital) apatite, and to visualise detrital apatite compositions versus the composition of apatite of known provenance (O'Sullivan *et al.*, 2018). Specifically, classification is carried out in Sr/Y vs ΣLREE (sum of La, Ce, Pr and Nd) space.

Results

Field sedimentology

The MSFm is a fluvial/shallow marine clastic sequence which was deposited in a marine-dominant, coastal system. Stratigraphic relationships vary across locations with the western sections (locations

1 & 2) underlain by limestone formations while sections 3, 4a & 4b are underlain by the Bundoran Shale formations (Fig. 4).

Location 1, Bunatrahir West. The most westerly outcrop of the MSFm at Bunatrahir West (location 1; Fig. 2a) occurs NNW of Stella Maris Pier. The section is positioned stratigraphically above the Moyny Limestone Formation and approximately 57m of the lower part of the MSFm is exposed. An influx of clastic material is represented by an erosive base of the first MSFm channel sandstone, and a 10m sequence of stacked channel sandstones. The channel sandstones are medium-grained feldspathic, light-grey and thick-bedded, often with erosive bases and may also contain dewatering structures. Interbedded siltstones and sandstones, along with carbonate horizons (including calcilutites [micrites] and calcareous sandstones) are also present; however, the channel sandstone facies is very prominent in the sequence. Fossil plant material (chiefly *Lepidodendron*) is common throughout and in-situ rootlets are also present at some horizons. Marine fossils preserved in a carbonate nodule in one discrete bed included crinoids, corals, bryozoans, goniatites and conodonts, the latter indicating a Viséan age.

Location 1 includes the only conglomerate bed observed in the MSFm, located directly below a channel sandstone and containing imbricated clasts of schist, gneiss, siltstone and vein quartz (pebble and cobble grades). A distinctive feature at this location is the presence of inclined heterolithic strata. Three discrete packages of this facies are evident, and they are interpreted as large-scale bar structures which are the remnants of meandering tidal creeks.

Location 2, Kilcummin. This locality is 11.5km east of location 1 (Fig. 2a), and approximately 76m from the upper part of the MSFm is exposed. In contrast to location 1, this section has less of a fluvial influence and is more marine in character, with brachiopods, corals (solitary and colonial), crinoids and bryozoans observed. Interbedded siltstones and sandstones, limestones, and calcareous sandstones are dominant at the base of the section, becoming coarser and more sand-rich towards the top of the sequence. The channel sandstone is laterally continuous and cross bedded. Location 2

is also extremely rich in trace fossils, principally representing the *Skolithos* and *Cruziana* ichnofacies (reflecting moderate-high and low-moderate energy, respectively ((Frey *et al.*, 1990; MacEachern *et al.*, 2012), with ichnogenera such as *Chondrites*, *Thalassanoides* and *Rhizocorallium* widespread.

Location 3, Carrowmoran. This locality is approximately 30km east of location 1 (Fig. 2b) and presents the most complete section through the MSFm, with 84m exposed. Both the base and top of the formation are exposed (with just ~2m section missing in the middle) and a gradual transition from the underlying Bundoran Shale Formation to the MSFm is evident. Thick channel sandstones occur throughout and display erosive bases and sedimentary structures indicative of significant dewatering and fluidisation (such as convoluted bedding, slumping, dish structures, sand nodules or 'pseudonodules' and sand volcanoes). These are likely associated with rapid sedimentation rates. Plant debris and rootlets also occur within the channel sandstones. Interbedded siltstones and sandstones, mudstones, limestones and rippled sandstones occur between channel sandstones and bioturbation is common in the mudstone beds near the base of the sequence. A thick feldspathic channel sandstone was collected (sample 3) in the top half of the sequence at location 3.

Location 4a and 4b, Bundoran. These localities are the most northeasterly sections of the MSFm examined and are located approximately 60km east of location 1 (Fig. 2c). The base of the unit is exposed here and is erosive, with at least 1m of incision into the underlying Bundoran Shale Formation. The MSFm section at location 4a continues westwards around Mullaghmore Head and although much faulted, moves stratigraphically upwards where a topmost bed was sampled at location 4b (Fig. 2c). The section is exposed on a headland with a 7m vertical cliff section of multi-storey channel sandstones. This section contains abundant plant debris, bioturbation, dewatering structures and pseudonodules. The latter are load structures formed by soft sediment deformation and can be attached to a formative horizon above or become detached pseudonodules. Once several pseudonodules are stacked vertically in one section, they are termed ball and pillow

structures (Owen, 2003). Location 4b section also contains conspicuously coarse grains, in one location up to pebble-grade within the channel sandstone facies.

Petrography

Basal channel sample 4a is a subarkosic arenite while all other samples are defined as feldspathic arenites after (Pettijohn *et al.*, 1987). Quartz, K-feldspar (orthoclase, microcline, perthite) and plagioclase are the most abundant framework minerals, and some muscovite and very minor biotite is also present (Fig. 6). Sample 1 is extremely feldspar rich, containing a modal abundance of 58% feldspar, of which orthoclase is by far most common, followed by microcline, plagioclase and perthite. All other samples vary in feldspar modal abundance from 38% - 23%. Quartz is least common at location 1 with 39% modal abundance compared to 71% - 55% in all other samples. Plagioclase is subordinate to K-feldspar in all samples. Detrital igneous rock fragments are a minor component in the basal channel sandstones at locations 1 and 2, and also the representative top channel at location 3. Rock fragments are mainly comprised of fine-grained felsic clasts and microcrystalline quartz. The basal and topmost channel sandstones at locations 4a and 4b respectively contain comparatively more detrital igneous clasts, with those of a granitic composition most common. The various sampled sandstones (Table 2) are moderately sorted, with the exception of location 4a, where poor sorting is evident. Calcite cement is present in sample 2 (11%) and most notably in sample 4a with 27%.

Single grain provenance analysis

Pb-in-K-feldspar

Five samples with a total of 191 K-feldspar grains were analysed. These data are compared to a dataset of potential source terranes in the North Atlantic Region (Tyrrell *et al.*, 2007) on a $^{207}Pb/^{204}Pb$ versus $^{206}Pb/^{204}Pb$ plot (Fig. 7). Five distinct populations, corresponding to discrete sources, are evident across all samples (see also Table 3):

- The least radiogenic grains; *Fpop1a*, appear to correspond with the Pb domain typical of the Nagssugtoqidian.
- *Fpop1b* appears to correspond the Lewisian Complex / Stanton Banks.
- *Fpop2a* corresponds with Paleoproterozoic basement terranes offshore Ireland and Scotland, such as the Porcupine Bank, Rockall Bank and Rhinns Complex.
- *Fpop2b* corresponds with the Annagh Gneiss Complex.
- *Fpop3*, the most radiogenic detrital grains, strongly correlate with Caledonian Granites such as those in Donegal.

Data shows significant variability across the locations. Notably, feldspar from sample 1 comprises the most unique and distinct Pb isotopic population, suggestive of a single source corresponding with the *Fpop2a* and *Fpop2b* array, with a minor *Fpop3* component present. Sample 2 displays a more mixed detrital population with clusters of *Fpop1a*, *Fpop2a, Fpop2b*, and *Fpop3*. *Fpop4*, a very radiogenic population of unknown affinity is unique to Sample 2 and is not observed in any other sample.

Detrital K-feldspars from sample 3 are dominated by grains from *Fpop1a* and *Fpop1b*. There are two distinct populations present in the *Fpop2* domains, and also some minor *Fpop3* grains.

The most eastern basal channel sample of the MSFm at location 4a is again unique, in that it contains an array of compositions from *Fpop1a*, some *Fpop2a* and a dense cluster of *Fpop2b*. *Fpop3* grains are also present. There is only one outlying grain that corresponds to *Fpop1b*. This pattern changes in sample 4b, which displays a very broad detrital source signal from all of the defined populations, with dominance of the least radiogenic parts of *Fpop1a* and *Fpop1b*.

U-Pb Zircon Geochronology

Five samples, totalling 432 concordant zircon grains, were analysed and plotted as Kernel Density Estimates (KDEs) in the program R. A bin size of 30 Ma was selected based on the typical zircon age

uncertainties and the KDEs were overlain with age bands for ease of population identification (Fig. 8; table 3). On this basis, three distinct age populations were distinguished: *Zpop1*, with U-Pb ages >1.8 Ga; *Zpop2* (1.8-0.9 Ga); and *Zpop3* (490-370 Ma).

All of the samples have varying amounts of Archean zircons (*Zpop1*), characterised primarily by a peak at 2.75 Ga. However, all analysed samples are dominated by Paleo – Mesoproterozoic zircons (*Zpop2*), generally spanning from 1.75 – 0.95 Ga, with major peaks at 1.75 Ga, 1.65 Ga and 1.05 Ga and some at 1.45 Ga. The third and youngest population (*Zpop3*) corresponds with ages of the Caledonian Orogenic Cycle (Ordovician – Lower Devonian) and zircon derived from these events are found in variable proportions at each location.

Sample 1 is overwhelmingly dominated by a zircon U-Pb age peak of 1.75 Ga, with other very minor *Zpop2* peaks at 1.45 Ga and 1.05 Ga. By contrast, the other four samples display a wider spread of zircon ages. Sample 2 is dominated by slightly younger *Zpop2* grains (~1.65 Ga). 1.75 Ga and 1.05 Ga grains are also abundant, along with *Zpop3* and *Zpop1* grains. Sample 3 has a very similar detrital zircon profile to sample 2, the only difference being slightly less *Zpop3* and *Zpop2* grains. Sample 4a has minor *Zpop1* and *Zpop3* components and is also dominated by *Zpop2* material. The majority of grains are 1.65 Ga with a lesser 1.75 Ga population. 1.2-1.05 Ga grains are also evident. Sample 4b, the topmost channel in the MSFm, shows some differences with a relatively elevated *Zpop3* component and a relative paucity of the 1.2 Ga population and with the *Zpop1* component also slightly elevated compared to other samples.

U-Pb Apatite geochronology

Five samples and a total of 471 grains were analysed, of these 320 grains yielded ^{207}Pb-corrected ages which passed the age uncertainty threshold, and these were plotted on KDEs with a bandwidth of 30 Ma alongside the zircon data (Fig. 8). Three main grain populations were identified; *Apop1* with U-Pb ages (>1.8 Ga); *Apop2* (1.8-0.9 Ga); and *Apop3* (490-370 Ma) (Table 3).

Apop1 is present only as a very minor component, these apatite have ages in the range of 2.0 - 1.8 Ga. *Apop2* encompasses the widest interval of geological time and varies between all samples. Prominent age peaks are evident at 1.75 Ga and 1.65 Ga (particularly in samples 1 & 4b) and minor peaks are also present at 1.55 Ga, 1.45 Ga, 1.35 Ga, and 1.05 Ga (Fig. 8). *Apop3* is very prominent and well-defined in all samples except sample 1.

Sample 1 has a unique U-Pb apatite grain population, almost entirely comprising *Apop2*. While a 1.75 Ga component is present, the younger 1.65 Ga population is most abundant in this sample. In comparison, the other four samples are composed predominantly of *Apop3* grains. Sample 2 also contains a range of *Apop2* at 1.7 Ga, 1.6 Ga and 1.1 Ga. Sample 3 and 4 also contain a sub-population of the *Apop2* component, the latter sample displaying minor peaks at 1.75 Ga and 1.45 Ga. Sample 4b displays an *Apop2* peak at 1.75 Ga and another at 1.6 Ga.

Trace elements in apatite

Trace element data from 454 apatite grains are plotted on a Sr/Y *vs* LREE biplot against a lithological categorisation scheme established from apatite of known composition (O'Sullivan *et al.*, 2020). Pie charts are used to visualise the proportion of detrital apatite plotting in each lithology field (Fig. 9). The lithological groupings are: LM (apatite from low and medium grade metamorphic and metasomatic rocks); I+M (I-type granitoids and mafic igneous); HM (high grade metamorphic); UM (ultra-mafic igneous); and negligible amounts of S (S-type granitoids) and ALK (alkali-rich igneous). The majority of grains which did not yield acceptable U-Pb age uncertainties (~32% of all apatite analysis) plot in the field defined by 'LM' apatite. This is similar to the findings of (O'Sullivan *et al.*, 2020), wherein 'LM' apatite is shown to be significantly more U-poor than apatite from other lithology groupings.

Sample 1 is again distinct with 76% of grains of I+M type, compared to 8-27% in the other samples. It contains only 4% of grains of LM affinity compared to 53-67% in all other samples. Apatite of HM

affinity ranges between 8-22% in all sections. Interestingly, although few apatite plot in the UM field (2-3%) in sample 1, samples 4a (14%) and 4b (7%) contain significantly more apatite grains with geochemical affinity to UM apatite (which is defined by apatite from harzburgites, lherzolites, pyroxenites and carbonatites).

When apatite geochronology is coupled with trace element data (Fig. 10), the trends indicate that metamorphic grains (LM and HM) are most common in the Paleozoic grain populations, but also from 1.7–1.0 Ga. I+M type sources are also found in the Paleozoic grain population but are most abundant in the Paleoproterozoic population, especially at peaks 1.75 Ga and 1.65 Ga. Grains of UM affinity are restricted to Paleozoic-aged grains.

When considering only the Paleozoic grains in detail (Fig. 10b), the LM peak yields ages of 450 Ma. Grains of I+M affinity have ages of 445–425 Ma, with a peak that overlaps with the largest HM peak at 435 Ma, which also has minor peaks at c. 450 Ma and 490 Ma. Grains of UM affinity define the youngest population at 420–415 Ma.

Discussion

Provenance of the Mullaghmore Sandstone Formation

The MSFm is composed of detrital grains sourced from various terranes in the NE Atlantic region (Fig. 11). The oldest (determined by U-Pb zircon geochronology) and least radiogenic sources (determined by Pb-in-feldspar analysis) correspond to Archean–Paleoproterozoic rocks (2.75–1.8 Ga). Pb-in-K feldspar data enable discrimination between the similarly aged Nagssugtoqidian (*Fpop1a*) and the Lewisian Complex (*Fpop1b*).

All grains associated with *Pop2* are Paleo – Mesoproterozoic, yielding zircon and apatite U-Pb ages between 1.79–0.98 Ga. Most notable are zircon age peaks at 1.78, 1.65, 1.45 and 1.1 Ga – which are all related to orogenic events and major igneous activity in the present North Atlantic region, such as:

- major igneous activity in what is now the north Atlantic region from 1.9–1.7 Ga (Daly, 1996; Morton et al., 2009; Scanlon et al., 2003a; Stephenson et al., 2013)
- Labradorian events between 1.6–1.4 Ga (Morton and Taylor, 1991),
- Pinwarian events between 1.51–1.45 Ga (Gower and Krogh, 2002; Augland *et al.*, 2015) and
- Grenville orogenesis between 1.3-1.0 Ga (McLelland *et al.*, 1996).

Detrital Pb-in-K-feldspar analysis helps further pinpoint these *FPop2a* sources as offshore highs, such as Rockall and Porcupine Banks, as well as the Rhinns Complex. *Fpop2b* is distinguishable and is representative of material sourced from the Annagh Gneiss Complex onshore western Ireland.

The third and youngest population (*Pop3*) corresponds with rocks associated with the Caledonian Orogenic Cycle and yields U-Pb zircon ages of 475–390 Ma. Granitic intrusions associated with the Donegal batholith yield U-Pb zircon ages ranging from 430 – 400 Ma (Archibald *et al.*, 2021). Pb-in-K-feldspar data (Fig. 7) also suggests sourcing of feldspar grains from Donegal Granites and, potentially, along-strike equivalents, which would also be a source for the younger Caledonian (420 – 400 Ma) zircons and igneous apatites.

Trace elements in apatite combined with apatite U-Pb geochronology (Fig. 10) is a powerful provenance tool as it combines source lithology information with a medium temperature thermochronometer. Apatite has a U-Pb closure temperature of 375–550°C (Cochrane *et al.*, 2013) meaning that the U-Pb system in apatite will likely be reset if these temperatures are exceeded. In the Grampian Orogen this temperature range (broadly corresponding to the upper greenschist to lower-amphibolite facies) would have been exceeded throughout much of the orogenic belt based on the regional metamorphic grade (Stephenson *et al.*, 2013). Moreover, apatite is a reactive mineral phase in metamorphic systems, and commonly experiences dissolution-reprecipitation reactions at temperatures below the nominal closure temperature of its U-Pb system (Harlov *et al.*, 2005; Henrichs *et al.*, 2018).

When isolating Caledonian-aged apatite from the dataset, the grain count (n) notably reduces, however useful information can still be garnered from these data. The Early Paleozoic low- to medium-grade metamorphic apatite population (LM) (Fig. 10 b (i)) is almost certainly derived from the Grampian Belt, with the main c. 450 Ma peak representing cooling from the c. 475-465 Ma Grampian orogenic peak (Dewey, 2005; Chew, 2009) and the slightly older ages representing primary crystallization ages in the lower greenschist-facies portion of the orogen. The similar pattern (but inverted with respect to relative abundance of age peaks) in the high-grade metamorphic spectrum (Fig. 10 b (ii)) is interpreted to have a similar origin. These metamorphic populations are not represented in zircon data, as zircon formation is restricted in regional metamorphic belts which do not culminate in anatexis (Moecher and Samson, 2006).

I-type granitoids and mafic igneous sources of apatite are also common in the Caledonian Orogenic Belt, especially between 440–420 Ma, suggesting a primary igneous source for these grains. While the c. 430 Ma HM peak could be attributed to the Scandian phase of the Caledonian Orogenic Cycle which reached temperatures of 700 °C and up to eclogite facies metamorphism in the Northern Highland Terrane, NW Scotland (Strachan *et al.*, 2020), it should be noted that some of this prominent HM apatite peak (coeval with the IM apatite population) could also represent S-type granitoid apatite, as the apatite source rock classification approach of O'Sullivan et al. (2020) is least able to discriminate between high-grade metamorphic rocks and S-type granitoids, as the former may have experienced anatexis and thus share common petrogenetic features with the latter. The c. 420-415 Ma UM apatite peak likely represents the Caledonian appinite-lamprophyre suite. Small clusters and pipes of ultramafic dykes (pyroxene, hornblende and amphibole rich) are a common feature in the Caledonian Orogenic Cycle of Ireland and Britain (Fowler and Henney, 1996). These formed as a result of the closure of the Iapetus Ocean in the Silurian, where subduction lead to slab break off and the upwelling of the aesthenosphere (Murphy, 2013; Murphy, 2019). In Donegal (northwest Ireland), these ultramafic dyke swarms intrude into the Dalradian Supergroup (Archibald *et al.*, 2021).

The Caledonian Orogenic cycle U-Pb peaks (*Zpop3* and *Apop3)* thus comprise two main components. Late Caledonian granitoids and associated intrusives comprise *Zpop3* and the apatite c. 430 Ma I+M and 420-415 Ma UM populations. The older (c. 490 – 450 Ma) LM and HM apatite populations in *Apop3* represent either primary metamorphic apatite (re)crystallization of the Grampian orogen, or cooling ages from the c. 475-465 Ma Grampian orogenic peak. No apatite derived from Grampian igneous sources, the dominant signal in Ordovician sediments 50km to the Southwest of the study area, are reported (O'Sullivan and Chew, 2020).

These analytical data are in direct agreement with sedimentological provenance data from the conglomerate bed near the top of the sequence at location 1. Schist pebbles likely derive from the Dalradian Supergroup while the gneiss pebbles are likely sourced from the Annagh Gneiss Complex.

Spatial variation in provenance signal in the MSFm

The channel sandstone at location 1, the most westerly sampled section, yields a very different provenance signal to all other samples, which is a consistent observation across all proxies. It displays a unimodal source with a *Zpop2* peaking at 1.75 Ga and subordinately at 1.05 Ga, typical of the Annagh Gneiss Complex (AGC; Figure 4). The Pb-in-K-feldspar data exhibits a tight distribution across *Fpop2*, suggestive of a single AGC source, consistent with the U-Pb zircon data. The apatite U-Pb data reveal a minor peak at 1.75 Ga and a major peak at 1.65 Ga, while the apatite trace element data suggest only 25% of grains are of metamorphic origin with the majority of grains derived from I-type granitoids and / or mafic igneous rocks. As the AGC bedrock in NW Ireland yields Grampian U-Pb ages (Henrichs *et al.*, 2018), an AGC-type igneous terrane which has not experienced the Caledonian orogenic cycle is a potential source. Additionally, apatite, zircon and K-feldspar associated with *Pop1* and *Pop3* are present in negligible amounts in this sample. It is therefore proposed that an AGC equivalent (now offshore and to the north of the Grampian and Grenville orogenic belts) was the sole contributor of detritus to the MSFm at location 1.

Zircon geochronological data from all other locations are broadly similar, however, the relative proportion of each of the identified populations varies. *Zpop1* is most prominent at location 2. *Zpop3* increase in abundance from locations 2 to 4a and is most abundant at 4b, implying that input from Caledonian plutonic sources increases in the MSFm north-eastwards. 1.75 Ga zircon components are subordinate to 1.65 Ga components in all samples except at location 3.

The Caledonian *Apop3* population is broadly consistent in all other samples (except sample 1), *Apop1* is minor while *Apop2* demonstrates the most variability across samples. The lack of Archean-aged apatite grains is likely related to recrystallization or U-Pb age resetting during subsequent metamorphic events. It has previously been noted that detrital apatite older than 2 Ga derived from the Lewisian terranes in NW Scotland is proportionately rare (Kenny *et al.*, 2019). Location 4b, the most northerly section, exhibits a notably different *Apop2* population. A pronounced 1.75 Ga apatite age population is present compared to other samples, with a minor 1.65 Ga component. As this is the youngest of the sampled channel sandstones, the source signal at location 4b has perhaps been most influenced by subsequent hinterland development as the fluvial system eroded deeper into bedrock or expanded its catchment. The apatite trace element data show little variation, with the exception of a minor increase in ultramafic sourced apatite at locations 4a and b. This is likely linked to the Caledonian ultramafic appinite-lamprophyre suite and is potentially being sourced from such rocks in Donegal (Bowes, 1989; Murphy, 2019). These sources are volumetrically small, and hence only contribute relatively few grains, but are likely more abundant in the north-easternmost sandstone sample due to their relative proximity to these sources (Fig. 1).

The Pb-in-K-feldspar data shows slightly more variation across the sample locations (Fig. 7). *Fpop1a* (corresponding to the Nagssugtoqidian) appears to be a consistent sediment contributor. *Fpop1b* (corresponding to a Lewisian / Stanton Banks source) is present in detritus from locations 3 and 4b, while almost absent at locations 2 and 4a. The Paleoproterozoic *Fpop2a* and *Fpop2b* populations contributed equally at location 2 and 4b, whereas locations 3 and 4a have a higher abundance of

Fpop2a and *Fpop2b* populations. *Fpop3* (Caledonian-affinity feldspar) is present to a minor extent in all samples with slightly increased abundance at locations 4a and 4b – suggesting increased sourcing from Donegal Granites and agreeing with the increased input of ultramafic apatite (see above). *Fpop4*, for which there is no currently known source, is only present at location 2. This cryptic population could represent a local, volumetrically minor (and presumably young) igneous rock, potentially exposed along strike within the GGF fault zone off the coast of NW Ireland.

All detrital proxies reveal the basal MSFm channel at location 1 is conspicuously different from the basal channel sampled at location 4a, and the higher-level channel sandstones from locations 2, 3 and 4b. This suggests that the fluvial system, as recorded at location 1, was either i) not linked to the fluvial systems supplying the other sample locations *or* ii) represents an earlier channel system at the initiation of clastic input that later gets captured.

Sedimentary Recycling

The recycling of detrital grains from sedimentary or metasedimentary rocks is a common problem faced in provenance studies, as if it goes unrecognised, it can lead to erroneous interpretations of sediment pathways. This phenomenon most commonly impacts U-Pb zircon data as it is a robust mineral phase which is able to survive multiple episodes of sedimentary recycling (Morton, 1984). The supply of recycled material to the NWCB has been constrained in this study using multiple proxies. The metasedimentary Dalradian Supergroup formed on the southern margin of Laurentia andsourced the interior of the Laurentian Continent (Cawood *et al.*, 2003). This 'primary source' subsequently experienced metamorphism during the Grampian phase of the Caledonian Orogenic Cycle. Many source areas associated with the ancient continent of Laurentia yield Paleo – Mesoproterozoic zircon ages from 1.8 – 0.98 Ga, often having similar crystallisation ages (e.g. 1.75 Ga; Rhinns Complex, Rockall Bank, Annagh Gneiss Complex) and thus this age component is particularly abundant. The apatite U-Pb and trace element data reveal that almost 50 % of sampled apatite grains yield ages corresponding to the Caledonian Orogenic Cycle and have compositions

characteristic of apatite from low-grade metamorphic rocks (e.g. Henrichs *et al.*, 2018; O'Sullivan *et al.*, 2020). These are likely sourced from the regionally extensive Dalradian Supergroup low-grade metasedimentary rocks. Assuming that apatite and zircon source fertility was comparable, this indicates that a potentially significant proportion of zircon must also be recycled from Dalradian metasedimentary rocks; in particular, much of the Proterozoic (and potentially some of the Archean) population (Cawood *et al.*, 2003). Comparison of detrital zircon age ranges from the Dalradian Supergroup (albeit from Scotland) with those from the MSFm (Fig. 12) show clear similarities, supporting the idea that a portion of the MSFm was recycled from this metasedimentary succession. The Pb-in-K-feldspar tool further helps constrain recycling issues. K-feldspar is unlikely to survive sedimentary recycling (Johnson *et al.*, 2018), hence it likely reveals first cycle input from each terrane, dependent, of course, on relative K-feldspar fertility (see below).

Apatite has been similarly regarded as a likely first cycle component, as it is susceptible to breakdown under conditions of acidic chemical weathering at the surface. However, unlike feldspar, apatite is resistant to breakdown during burial diagenesis. However (Nauton-Fourteu *et al.*, 2020) have demonstrated that, in specific circumstances, significant apatite can survive more than one sedimentary cycle. Original apatite U-Pb ages, however, may be overprinted and reset by regional metamorphism associated with orogenesis, technically yielding it a (re)crystallised metamorphic grain. However, by default recycled populations may be identified. This has proven to be a particularly useful feature in this study of the MSFm, as only the apatite data is recording the sourcing from metamorphic terranes (O'Sullivan *et al.*, 2016). These would go unrecognised if the study relied on zircon and feldspar data alone.

Fertility

The use of a multi proxy approach helps constrain another common problem faced in provenance studies - the biases introduced by variable source fertility (Flowerdew *et al.*, 2019; Chew *et al.*, 2020). Besides the dominant 1.8-1.7 Ga zircon U-Pb age component, the 1.3-1.0 Ga peak is the

second most abundant age population in the zircon U-Pb data (Fig. 8). This population is associated with the Grenville Orogeny (Daly, 2009) and the intensity of its signal is likely due to the unusually high zircon yield in Grenville magmatic provinces (rather than a function of a high volume of sediment input from this source). For example, granitic Grenville terranes yield a higher proportion of zircon than Paleozoic granites in the Appalachians (Moecher and Samson, 2006).

Using multiple proxies and various mineral species such as stable zircon and relatively labile K-feldspar and apatite, allows for ultramafic and mafic sources to be identified, which may be overlooked when using zircon as a sole proxy (Garzanti and Andò, 2019). It is evident from apatite data that ultramafic rocks appear to provide a 420 – 415 Ma (late Silurian – early Devonian) grain population. Ultramafic rocks are very poor in both zircon and K-feldspar, hence sourcing from these rocks would not have been recognised without the specific use of apatite.

While a source for metamorphic apatite, and likely a portion of the recycled zircon, the Dalradian Supergroup clearly cannot be the exclusive source of these minerals, or for K-feldspar. The apatite trace element data clearly highlights the presence of Caledonian-aged igneous apatite, apatite U-Pb ages data rules out a Grampian-Taconic magmatic arc source (cf. (O'Sullivan and Chew, 2020). K-feldspar is not likely to survive multiple sedimentary cycles (Tyrrell *et al.*, 2010) and the Dalradian Supergroup thus cannot be the source for the large (> 1 cm) K-feldspars found at locations 1 & 4a (which samples have up to 25% K-feldspar modal composition), indeed the rocks of the Dalradian Supergroup are known to contain little K-feldspar (Woodcock and Strachan, 2009; Johnson *et al.*, 2016). These K-feldspar grains are likely sourced from high grade gneisses such as the Annagh Gneiss Complex or the Caledonian Granites of Donegal.

Single grain double proxy approach: apatite as a provenance tool

Apatite has been used commonly for fission track dating and to determine exhumation history of rocks (Dunkl, 2002). Recently, it has also gained popularity for combined U-Pb dating and trace

element analysis (O'Sullivan *et al.*, 2018; Franklin *et al.*, 2019; Nauton-Fourteu *et al.*, 2020; O'Sullivan *et al.*, 2020). This ubiquitous mineral is an extremely useful provenance proxy as it helps address common issues such as recycling, which are often unaccounted for in provenance studies reliant on zircon geochronology alone. Additionally, when trace element data are combined with U-Pb age data the age and lithological source type of the apatite can readily be identified (e.g. Fig. 10), which helps constrain the relative abundance of recycled grains.

When considering the most recent orogenic episode in the hinterland, the Ordovician – late Silurian Caledonian Orogenic Cycle, individual phases within this orogenic cycle may be distinguished in the apatite data. Despite a relative low grain count some clear trends are evident. High-grade metamorphism was more frequently attained during the Scandian Orogeny (437 - 415Ma) which reached eclogite facies conditions (Strachan *et al.*, 2020), but is spatially restricted to zones in northern Scotland, East Greenland and the Scandinavian Caledonides. Low-medium grade metamorphic apatite is most evident in the Ordovician and is associated with the 475 – 465 Ma Grampian Orogeny. The older (c. 490- 465 Ma) LM and HM apatite populations likely represent primary metamorphic apatite crystallization in the Grampian orogen while the younger (c. 450 Ma) metamorphic apatite represents Grampian cooling ages or possibly 450 Ma metamorphism reported from the NW Highlands terrane (e.g., Bird *et al.*, 2013)). The youngest c. 430 Ma HM apatite population could either represent long cooling times from peak Grampian conditions or potentially represent grains deriving from the Scandian phase of the Caledonian Orogenic Cycle. Thus, apatite not only has the capacity to identify the Dalradian Supergroup as a source, it also has the potential to identify sourcing from discrete parts of this metasedimentary belt.

Conclusions

This study highlights spatial variation in provenance signal within the Viséan Mullaghmore Sandstone Formation, a widely correlatable, clastic-dominated lithostratigraphic unit within the modest sized North-West Carboniferous Basin (NWCB) in north-western Ireland. These provenance data unveil the

cryptic origin of detritus across the basin and its relationship to distinct localised paleodrainage patterns. The basal channel sandstone at location 1 appears to be sourced from a single discrete terrane (a point source) interpreted as an offshore correlative of the Annagh Gneiss Complex. In contrast, the basal channel sandstone at 4a and all other sampled channel sandstones, show more variable detritus from a much wider and geologically diverse catchment/hinterland, which we interpret as sourced from the north and northwest. This suggests that at least during onset of clastic sedimentation the fluvial system feeding location 1 was distinctly different to the fluvial system feeding the other locations. It is possible that evolution and development of the sediment routing system may have connected these smaller systems at a later stage. The MSFm at location 2 has a significant marine influence and displays a very mixed detrital signal, further emphasising the important role that sedimentology and facies analysis must play in the interpretation of provenance signals in complex sediment routing systems when supply varies at individual positions within a single basin.

Results from this study highlight the importance of adopting a multiproxy provenance approach. An effective method combines a tool based on a combination of both robust and less-stable mineral proxies (such as zircons and feldspar/apatite, respectively). The durability of zircon ensures that no source component is overlooked, and it provides accurate crystallisation ages of the source terranes, while the feldspar tool helps separate certain source areas that yield similar U-Pb ages, but differing Pb isotopic ratios. . This study reveals the Dalradian Supergroup as a potentially significant source for recycled zircon, demonstrating that our approach can help address some of the common biases and issues introduced by phenomenon such as sedimentary recycling and variations in mineral source fertility.

Detrital apatite geochronology appears to accurately record the last metamorphic event experienced in the sourcelands, as the U-Pb system is reset/overprinted. In addition, apatite trace element data can differentiate between different types of metamorphic and igneous apatite

(O'Sullivan *et al.*, 2020), a useful tool as metamorphic belts can be identified and tracked as possible sources, while various plutonic phases can be fingerprinted. Furthermore, sourcing from various discrete parts of metamorphic belts may be identified (e.g. Grampian Belt) with a joint apatite U-Pb and trace element approach, yielding much more information than dating alone.

Any tool used in isolation can lead to interpretations and models that are inaccurate or erroneous. The power of provenance analysis to reveal genuine insight into ancient sedimentary systems is greatly enhanced with a bespoke multi-proxy approach, and complex sediment pathways can be unravelled.

Acknowledgements

Special thanks to C. Reid and L. O'Connor (iCRAGlabs@TCD) and J.S. Daly (National Centre for Isotope Geochemistry, NCIG, UCD) for technical assistance. Two anonymous referees and associate editor Prof Martin Whitehous are acknowledged for their helpful comments which improved this paper.

Funding

Funding for this research was obtained by through a Hardiman Scholarship from NUI, Galway, CASP fieldwork grant, a Thomas Crawford Hayes award (NUI Galway) and an International association of sedimentology (IAS) postgraduate grant. The original pilot study was funded by Geological Survey Ireland (GSI) (grant 2015-sc-029), under the "Geological Survey of Ireland Research Programme - Short Call Scheme". ST, DC and JM are partly supported by research grants from Science Foundation Ireland (SFI) under Grant Number 13/RC/2092 (iCRAG) which is co-funded under the European Regional Development Fund and by PIPCO RSG and its member companies. CM is funded by grant no. 18/SIRG/5559 from Science Foundation Ireland. The National Centre for Isotope Geochemistry (NCIG) is a joint venture of University College Dublin, Trinity College Dublin, University College Cork, and National University of Ireland Galway. NCIG was funded primarily by Science Foundation Ireland including grants 04/BR/ES0007/EC07 and 04/BR/ES0007S1 awarded to J.S. Daly (University College Dublin), who kindly provided access to analytical facilities for this project. E. B. was supported by Science Foundation Ireland grant 13/RC/2092, which is co-funded under the European Regional Development Fund. This grant also supported the purchase of the Teledyne Cetac G2 laser ablation system used in this study.

Author contributions

BA: Conceptualization (Lead), Data curation (Lead), Formal analysis (Lead), Investigation (Lead), Methodology (Lead), Funding acquisition (Lead) Writing – Original Draft (Lead); ST: Conceptualization (Equal), Funding acquisition (Equal), Investigation (Equal), Methodology (Equal), Project administration (Lead), Supervision (Lead), Writing – Review & Editing (Equal); DC: Formal

analysis (Supporting), Data curation (Supporting), Writing – Review & Editing (Supporting); JM: Writing – Review & Editing (Supporting); CM: Data curation (Supporting), Formal analysis (Supporting), Writing – Review & Editing (Supporting); GOS: Data curation (Supporting), Formal analysis (Supporting), Writing – Review & Editing (Supporting); JG: Investigation (Supporting); EB: Formal analysis (Supporting).

References

Archibald, D.B., Macquarrie, L.M. *et al.* 2021. The construction of the Donegal composite batholith, Irish Caledonides: Temporal constraints from U-Pb dating of zircon and titanite. *GSA Bulletin*, https://doi.org/10.1130/b35856.1.

Augland, L.E., Moukhsil, A., Solgadi, F. and Indares, A. 2015. Pinwarian to Grenvillian magmatic evolution in the central Grenville Province: new constraints from ID–TIMS U–Pb ages and coupled Lu–Hf S–MC–ICP–MS data. *Canadian Journal of Earth Sciences*, **52**, 701-721, https://doi.org/10.1139/cjes-2014-0232.

Barham, M., Murray, J., Joachimski, M. and Williams, D. 2012. The onset of the Permo-Carboniferous glaciation: reconciling global stratigraphic evidence with biogenic apatite δ18O records in the late Visean. *Journal of the Geological Society*, **169**, 119-122, https://doi.org/10.1144/0016-76492011-102.

Barham, M., Kirkland, C.L., Hovikoski, J., Alsen, P., Hollis, J., Tyrrell, S. and Tosca, N. 2020. Reduce or recycle? Revealing source to sink links through integrated zircon–feldspar provenance fingerprinting. *Sedimentology*, **68**, 531-556, https://doi.org/10.1111/sed.12790.

Bird, A., Thirlwall, M., Strachan, R. and Manning, C. 2013. Lu–Hf and Sm–Nd dating of metamorphic garnet: evidence for multiple accretion events during the Caledonian orogeny in Scotland. *Journal of the Geological Society*, **170**, 301-317, https://doi.org/10.1144/jgs2012-083.

Blakey, R.C. 2008. Gondwana paleogeography from assembly to breakup—A 500 my odyssey. *Geological Society of America Special Papers*, **441**, 1-28.

Blowick, A., Pe-Piper, G., Piper, D.J.W., Zhang, Y. and Tyrrell, S. 2020a. First-cycle sand supply and the evolution of the eastern Canadian continental margin: Insights from Pb isotopes in the Mesozoic Scotian Basin. *GSA Bulletin*, https://doi.org/10.1130/b35419.1.

Blowick, A., Pe-Piper, G., Piper, D.J.W., Zhang, Y. and Tyrrell, S. 2020b. First-cycle sand supply and the evolution of the eastern Canadian continental margin: Insights from Pb isotopes in the Mesozoic Scotian Basin. *GSA Bulletin*, **133**, 1301-1319, https://doi.org/10.1130/b35419.1.

Blowick, A., Haughton, P., Tyrrell, S., Holbrook, J., Chew, D. and Shannon, P. 2019. All mixed up: Pb isotopic constraints on the transit of sands through the Mississippi-Missouri River drainage basin, North America. *GSA Bulletin*, **131**, https://doi.org/10.1130/B35057.1.

Bowes, D. 1989. Appinite. *The Encyclopedia of Igneous and Metamorphic Petrology (Ed. Bowes, DR)*, 30-34.

Cawood, P.A., Nemchin, A.A., Smith, M. and Loewy, S. 2003. Source of the Dalradian Supergroup constrained by U–Pb dating of detrital zircon and implications for the East Laurentian margin. *Journal of the Geological Society*, **160**, 231-246, https://doi.org/https://doi.org/10.1144/0016-764902-039.

Chadwick, B. and Garde, A.A. 1996. Palaeoproterozoic oblique plate convergence in South Greenland: a reappraisal of the Ketilidian Orogen. *Geological Society, London, Special Publications*, **112**, 179, https://doi.org/10.1144/GSL.SP.1996.112.01.10.

Chew, D. 2009. Grampian Orogeny *The geology of Ireland*. Dunedin Academic Press,, 69-93.

Chew, D. and Stillman, C. 2009. Late Caledonian orogeny and magmatism. *In*: Holland, C. and Sanders, I. (eds) *The geology of Ireland*. Dunedin Academic Press Ltd, Edinburgh, 143-173.

Chew, D., Drost, K. and Petrus, J.A. 2019a. Ultrafast, > 50 HzLA-ICP-MSSpot Analysis Applied to U–Pb Dating of Zircon and other U-Bearing Minerals. *Geostandards and Geoanalytical Research*, **43**, 39-60, https://doi.org/10.1111/ggr.12257.

Chew, D., O'Sullivan, G., Caracciolo, L., Mark, C. and Tyrrell, S. 2020. Sourcing the sand: Accessory mineral fertility, analytical and other biases in detrital U-Pb provenance analysis. *Earth-Science Reviews*, **202**, 103093, https://doi.org/10.1016/j.earscirev.2020.103093.

Chew, D., Tyrrell, S., Daly, J.S., Cogné, N., Sun, K. and Badenszki, E. 2019b. The basement geology of the Porcupine High – A key transatlantic link between the Caledonides and Appalachians. *GSA*.

Chew, D.M. and Schaltegger, U. 2005. Constraining sinistral shearing in NW Ireland: a precise U-Pb zircon crystallisation age for the Ox Mountains Granodiorite. *Irish Journal of Earth Sciences*, 55-63.

Chew, D.M. and Strachan, R.A. 2014. The Laurentian Caledonides of Scotland and Ireland. *Geological Society, London, Special Publications*, **390**, 45-91, https://doi.org/10.1144/SP390.16
Chew, D.M., Sylvester, P.J. and Tubrett, M.N. 2011. U–Pb and Th–Pb dating of apatite by LA-ICPMS. *Chemical Geology*, **280**, 200-216, https://doi.org/10.1016/j.chemgeo.2010.11.010.
Chew, D.M., Petrus, J.A. and Kamber, B.S. 2014. U–Pb LA–ICPMS dating using accessory mineral standards with variable common Pb. *Chemical Geology*, **363**, 185-199, https://doi.org/10.1016/j.chemgeo.2013.11.006.
Chew, D.M., Babechuk, M.G. *et al.* 2016. (LA,Q)-ICPMS trace-element analyses of Durango and McClure Mountain apatite and implications for making natural LA-ICPMS mineral standards. *Chemical Geology*, **435**, 35-48, https://doi.org/10.1016/j.chemgeo.2016.03.028.
Clayton, G. 1985. Dinantian miospores and intercontinental correlation. *Congrès international de stratigraphie et de géologie du Carbonifère. 10*, 9-23.
Cochrane, R., Spikings, R.A. *et al.* 2013. High temperature (>350°C) thermochronology and mechanisms of Pb loss in apatite. *Geochimica et Cosmochimica Acta*, **127**, 39-56, https://doi.org/10.1016/j.gca.2013.11.028.
Connelly, J.N. and Thrane, K. 2005. Rapid determination of Pb isotopes to define Precambrian allochthonous domains: An example from West Greenland. *Geology*, **33**, 953-956, https://doi.org/10.1130/g21720.1.
Connolly, N. 2003. *Thesis. Sedimentology Analysis and Correlation of the Mullaghmore Sandstone Formation in the North and North-west of Ireland.* Trinity College Dublin.
Daly, J.S. 1996. Pre-Caledonian history of the Annagh Gneiss Complex North-Western Ireland, and correlation with Laurentia-Baltica. *Irish Journal of Earth Sciences*, 5-18.
Daly, J.S. 2009. Precambrian. *In*: In: Holland, C.H., Sanders, I.S. (Eds.) (ed.) *The Geology of Ireland.* . Dunedin Academic Press Ltd, Edinburgh, 7-42.
Davies, N.S. and Gibling, M.R. 2013. The sedimentary record of Carboniferous rivers: Continuing influence of land plant evolution on alluvial processes and Palaeozoic ecosystems. *Earth-Science Reviews*, **120**, 40-79, https://doi.org/10.1016/j.earscirev.2013.02.004.
Davies, S.J. and Fielding, C. 2008. The record of Carboniferous sea-level change in low-latitude sedimentary successions from Britain and Ireland during the onset of the late Paleozoic ice age *Resolving the Late Paleozoic Ice Age in Time and Space*. Geological Society of America Boulder, 187-204.
Deng, B., Chew, D. *et al.* 2021. Late Cenozoic drainage reorganization of the paleo-Yangtze river constrained by multi-proxy provenance analysis of the Paleo-lake Xigeda. *Bulletin*, **133**, 199-211, https://doi.org/10.1130/B35579.1.
Dewey, J.F. 2005. Orogeny can be very short. *Proceedings of the National Academy of Sciences*, **102**, 15286-15293.
Dickinson, W.R. 1988. Provenance and Sediment Dispersal in Relation to Paleotectonics and Paleogeography of Sedimentary Basins. *New Perspectives in Basin Analysis. Frontiers in Sedimentary Geology*, 3-25.
Dickinson, W.R. 2008. Impact of differential zircon fertility of granitoid basement rocks in North America on age populations of detrital zircons and implications for granite petrogenesis. *Earth and Planetary Science Letters*, **275**, 80-92, https://doi.org/10.1016/j.epsl.2008.08.003.
Dickinson, W.R., Lawton, T.F. and Gehrels, G.E. 2009. Recycling detrital zircons: A case study from the Cretaceous Bisbee Group of southern Arizona. *Geology*, **37**, 503-506, https://doi.org/10.1130/g25646a.1.
Ding, Z.L., Sun, J.M., Yang, S.L. and Liu, T.S. 2001. Geochemistry of the Pliocene red clay formation in the Chinese Loess Plateau and implications for its origin, source provenance and paleoclimate change. *Geochimica et Cosmochimica Acta*, **65**, 901-913, https://doi.org/10.1016/S0016-7037(00)00571-8.
Dunkl, I. 2002. Trackkey: a Windows program for calculation and graphical presentation of fission track data. *Computers & Geosciences*, **28**, 3-12, https://doi.org/10.1016/S0098-3004(01)00024-3.

Fielding, C.R., Frank, T.D. and Isbell, J.L. 2008. The late Paleozoic ice age—A review of current understanding and synthesis of global climate patterns *Resolving the late Paleozoic ice age in time and space*. Special Paper, 343-354.
Flowerdew, M.J., Tyrrell, S. and Peck, V.L. 2013. Inferring sites of subglacial erosion using the Pb isotopic composition of ice-rafted feldspar: Examples from the Weddell Sea, Antarctica. *Geology*, **41**, 147-150, https://doi.org/10.1130/g33644.1.
Flowerdew, M.J., Chew, D.M., Daly, J.S. and Millar, I.L. 2009. Hidden Archaean and Palaeoproterozoic crust in NW Ireland? Evidence from zircon Hf isotopic data from granitoid intrusions. *Geological Magazine*, **146**, 903-916, https://doi.org/10.1017/s0016756809990227.
Flowerdew, M.J., Fleming, E.J., Morton, A.C., Frei, D., Chew, D.M. and Daly, J.S. 2019. Assessing mineral fertility and bias in sedimentary provenance studies: examples from the Barents Shelf. *Geological Society, London, Special Publications*, **484**, SP484.411, https://doi.org/10.1144/sp484.11.
Fowler, M. and Henney, P. 1996. Mixed Caledonian appinite magmas: implications for lamprophyre fractionation and high Ba-Sr granite genesis. *Contributions to Mineralogy and Petrology*, **126**, 199-215, https://doi.org/10.1007/s004100050244.
Franklin, J., Tyrrell, S., Morton, A., Frei, D. and Mark, C. 2019. Triassic sand supply to the Slyne Basin, offshore western Ireland – new insights from a multi-proxy provenance approach. *Journal of the Geological Society*, jgs2019-2085, https://doi.org/10.1144/jgs2019-085.
Frey, R.W., Pemberton, S.G. and Saunders, T.D. 1990. Ichnofacies and bathymetry: a passive relationship. *Journal of Paleontology*, 155-158, https://doi.org/10.1017/S0022336000042372.
Gard, M., Hasterok, D. and Halpin, J.A. 2019. Global whole-rock geochemical database compilation. *Earth System Science Data*, **11**, 1553-1566, https://doi.org/10.5194/essd-11-1553-2019.
Garde, A.A., Hamilton, M., Chadwick, B., Grocott, J. and McCaffrey, K. 2011. The Ketilidian orogen of South Greenland: Geochronology, tectonics, magmatism, and fore-arc accretion during Palaeoproterozoic oblique convergence. *Canadian Journal of Earth Sciences*, **39**, 765-793, https://doi.org/10.1139/e02-026.
Garzanti, E. and Andò, S. 2007. Chapter 20 Heavy Mineral Concentration in Modern Sands: Implications for Provenance Interpretation. *In*: Mange, M.A. and Wright, D.T. (eds) *Developments in Sedimentology*. Elsevier, 517-545, https://doi.org/10.1016/S0070-4571(07)58020-9.
Garzanti, E. and Andò, S. 2019. Heavy Minerals for Junior Woodchucks. *Minerals*.
Gower, C.F. and Krogh, T.E. 2002. AU–Pb geochronological review of the Proterozoic history of the eastern Grenville Province. *Canadian Journal of Earth Sciences*, **39**, 795-829, https://doi.org/10.1139/e01-090.
Graham, J.R. 1996. Dinantian river systems and coastal zone sedimentation in northwest Ireland. *Geological Society, London, Special Publications*, **107**, 183, https://doi.org/10.1144/GSL.SP.1996.107.01.14.
Graham, J.R. 2010. The Carboniferous Geology of North Mayo. *Irish Journal of Earth Sciences*, **28**, 25-45.
Graham, J.R. 2017. The Mullaghmore Sandstone Formation of north-west Ireland: a regional Mississippian lowstand deposit. *Irish Journal of Earth Sciences*, **35**, 19-38, https://doi.org/10.3318/ijes.2017.35.19.
Graham, J.R. and Sevastopulo, G.D. 2020. The stratigraphy of latest Devonian and earliest Carboniferous rocks in Ireland. *Palaeobiodiversity and Palaeoenvironments*, 1-13, https://doi.org/10.1007/s12549-020-00455-y.
Guo, R., Hu, X., Garzanti, E., Lai, W., Yan, B. and Mark, C. 2020. How faithfully do the geochronological and geochemical signatures of detrital zircon, titanite, rutile and monazite record magmatic and metamorphic events? A case study from the Himalaya and Tibet. *Earth-Science Reviews*, **201**, 103082, https://doi.org/10.1016/j.earscirev.2020.103082.
Harlov, D.E., Wirth, R. and Förster, H.-J. 2005. An experimental study of dissolution–reprecipitation in fluorapatite: fluid infiltration and the formation of monazite. *Contributions to Mineralogy and Petrology*, **150**, 268-286, https://doi.org/10.1007/s00410-005-0017-8.

Hemming, S.R., McDaniel, D.K., McLennan, S.M. and Hanson, G.N. 1996. Pb isotope constraints on the provenance and diagenesis of detrital feldspars from the Sudbury Basin, Canada. *Earth and Planetary Science Letters*, **142**, 501-512, https://doi.org/10.1016/0012-821X(96)00102-1.
Henrichs, I.A., O'Sullivan, G., Chew, D.M., Mark, C., Babechuk, M.G., McKenna, C. and Emo, R. 2018. The trace element and U-Pb systematics of metamorphic apatite. *Chemical Geology*, **483**, 218-238, https://doi.org/10.1016/j.chemgeo.2017.12.031.
Higgs, K. 1984. Stratigraphic Palynology of the Carboniferous Rocks in Northwest Ireland. *Bulletin - Geological Survey of Ireland*, **3**, 171 - 202.
Hurst, A. and Morton, A. 2014. Provenance models: the role of sandstone mineral–chemical stratigraphy. *Geological Society, London, Special Publications*, **386**, 7-26, https://doi.org/10.1144/SP386.11.
Ibañez-Mejia, M., Pullen, A., Pepper, M., Urbani, F., Ghoshal, G. and Ibañez-Mejia, J.C. 2018. Use and abuse of detrital zircon U-Pb geochronology—A case from the Río Orinoco delta, eastern Venezuela. *Geology*, **46**, 1019-1022, https://doi.org/10.1130/G45596.1.
Johnson, S.P., Kirkland, C.L., Evans, N.J., McDonald, B.J. and Cutten, H.N. 2018. The complexity of sediment recycling as revealed by common Pb isotopes in K-feldspar. *Geoscience Frontiers*, **9**, 1515-1527, https://doi.org/10.1016/j.gsf.2018.03.009.
Johnson, T., Kirkland, C., Reddy, S., Evans, N. and McDonald, B. 2016. The source of Dalradian detritus in the Buchan Block, NE Scotland: Application of new tools to detrital datasets. *Journal of the Geological Society*, **173**, jgs2016-2019, https://doi.org/10.1144/jgs2016-019.
Johnston, S.M. and Kylander-Clark, A.R.C. 2013. Discovery of an Eo-Meso-Neoarchean terrane in the East Greenland Caledonides. *Precambrian Research*, **235**, 295-302, https://doi.org/10.1016/j.precamres.2013.07.004.
Kalsbeek, F., Nutman, A.P. and Taylor, P.N. 1993. Palaeoproterozoic basement province in the Caledonian fold belt of North-East Greenland. *Precambrian Research*, **63**, 163-178, https://doi.org/10.1016/0301-9268(93)90010-Y.
Kalsbeek, F., Frei, D. and Affaton, P. 2008. Constraints on provenance, stratigraphic correlation and structural context of the Volta basin, Ghana, from detrital zircon geochronology: An Amazonian connection? *Sedimentary Geology*, **212**, 86-95, https://doi.org/10.1016/j.sedgeo.2008.10.005.
Kelly, J.G. 1996. Initiation, growth and decline of a tectonically controlled Asbian carbonate ramp: Cuilcagh Mountain area, NW Ireland. *Geological Society, London, Special Publications*, **107**, 253-262, https://doi.org/10.1144/GSL.SP.1996.107.01.18
Kenny, G.G., O'Sullivan, G.J., Alexander, S., Simms, M.J., Chew, D.M. and Kamber, B.S. 2019. On the track of a Scottish impact structure: a detrital zircon and apatite provenance study of the Stac Fada Member and wider Stoer Group, NW Scotland. *Geological Magazine*, **156**, 1863-1876, https://doi.org/10.1017/S0016756819000220.
Kinny, P., Friend, C. and Love, G. 2005. Proposal for a terrane-based nomenclature for the Lewisian Gneiss Complex of NW Scotland. *Journal of the Geological Society*, **162**, 175-186, https://doi.org/10.1144/0016-764903-149.
Leeder, M. 1982. Upper Palaeozoic basins of the British Isles—Caledonide inheritance versus Hercynian plate margin processes. *Journal of the Geological Society*, **139**, 479-491, https://doi.org/10.1144/gsjgs.139.4.0479.
Leeder, M. 1987. Tectonic and palaeogeographic models for Lower Carboniferous Europe. *Geological journal. Special issue*, 1-20.
Leeder, M.R. 1988. Devono-Carboniferous river systems and sediment dispersal from the orogenic belts and cratons of NW Europe. *Geological Society, London, Special Publications*, **38**, 549-558, https://doi.org/10.1144/gsl.sp.1988.038.01.37.
Ludwig, K. 2012. User's Manual for Isoplot Version 3.75–4.15: A Geochronological Toolkit for Microsoft Excel. 5. *Berkley Geochronological Centre, Special Publication*.

MacDermot, C.V.L., C.B. and Harney, S.J. 1996. A geological description of Sligo, Leitrim, and adjoining parts of Cavan, Fermanagh, Mayo and Roscommon, to accompany the bedrock geology 1; 100,000 scale map series, sheet 7, Sligo-Leitrim. *The Geological Survey of Ireland*.
MacEachern, J.A., Bann, K.L., Gingras, M.K., Zonneveld, J.-P., Dashtgard, S.E. and Pemberton, S.G. 2012. The ichnofacies paradigm *Developments in sedimentology*. Elsevier, 103-138, https://doi.org/10.1016/B978-0-444-53813-0.00004-6.
Machado, N. and Gauthier, G. 1996. Determination of 207Pb/206Pb ages on zircon and monazite by laser-ablation ICPMS and application to a study of sedimentary provenance and metamorphism in southeastern Brazil. *Geochimica et Cosmochimica Acta*, **60**, 5063-5073, https://doi.org/10.1016/S0016-7037(96)00287-6.
Mark, C., Cogné, N. and Chew, D. 2016. Tracking exhumation and drainage divide migration of the Western Alps: A test of the apatite U-Pb thermochronometer as a detrital provenance tool. *Bulletin*, **128**, 1439-1460, https://doi.org/10.1130/B31351.1.
McAteer, C.A., Stephen Daly, J., Flowerdew, M.J., Connelly, J.N., Housh, T.B. and Whitehouse, M.J. 2010. Detrital zircon, detrital titanite and igneous clast U–Pb geochronology and basement–cover relationships of the Colonsay Group, SW Scotland: Laurentian provenance and correlation with the Neoproterozoic Dalradian Supergroup. *Precambrian Research*, **181**, 21-42, https://doi.org/10.1016/j.precamres.2010.05.013.
McDowell, F.W., McIntosh, W.C. and Farley, K.A. 2005. A precise 40Ar–39Ar reference age for the Durango apatite (U–Th)/He and fission-track dating standard. *Chemical Geology*, **214**, 249-263, https://doi.org/10.1016/j.chemgeo.2004.10.002.
McLelland, J., Daly, J.S. and McLelland, J.M. 1996. The Grenville Orogenic Cycle (ca. 1350-1000 Ma): an Adirondack perspective. *Tectonophysics*, **265**, 1-28, https://doi.org/10.1016/S0040-1951(96)00144-8.
Meyer, I., Davies, G.R. and Stuut, J.-B.W. 2011. Grain size control on Sr-Nd isotope provenance studies and impact on paleoclimate reconstructions: An example from deep-sea sediments offshore NW Africa. *Geochemistry, Geophysics, Geosystems*, **12**, https://doi.org/10.1029/2010GC003355.
Moecher, D.P. and Samson, S.D. 2006. Differential zircon fertility of source terranes and natural bias in the detrital zircon record: Implications for sedimentary provenance analysis. *Earth and Planetary Science Letters*, **247**, 252-266, https://doi.org/10.1016/j.epsl.2006.04.035.
Morrison, M.A., Hendry, G.L. and Leat, P.T. 2011. Regional and tectonic implications of parallel Caledonian and Permo-Carboniferous lamprophyre dyke swarms from Lismore, Ardgour. *Transactions of the Royal Society of Edinburgh: Earth Sciences*, **77**, 279-288, https://doi.org/10.1017/S0263593300023178.
Morton, A. 1984. Stability of detrital heavy minerals in Tertiary sandstones from the North Sea Basin. *Clay minerals*, **19**, 287-308.
Morton, A., Hitchen, K., Fanning, C., Yaxley, G., Johnson, H. and Ritchie, J. 2009. Detrital zircon age constraints on the provenance of sandstones on Hatton Bank and Edoras Bank, NE Atlantic. *Journal of The Geological Society - J GEOL SOC*, **166**, 137-146, https://doi.org/10.1144/0016-76492007-179.
Morton, A.C. and Taylor, P.N. 1991. Geochemical and isotopic constraints on the nature and age of basement rocks from Rockall Bank, NE Atlantic. *Journal of the Geological Society*, **148**, 631-634, https://doi.org/10.1144/gsjgs.148.4.0631.
Morton, A.C. and Hallsworth, C.R. 1999. Processes controlling the composition of heavy mineral assemblages in sandstones. *Sedimentary Geology*, **124**, 3-29, https://doi.org/10.1016/S0037-0738(98)00118-3.
Morton, A.C., Meinhold, G. *et al.* 2011. A heavy mineral study of sandstones from the eastern Murzuq Basin, Libya: Constraints on provenance and stratigraphic correlation. *Journal of African Earth Sciences*, **61**, 308-330, https://doi.org/10.1016/j.jafrearsci.2011.08.005.
Muir, R.J., Fitches, W.R. and Maltman, A.J. 1992. Rhinns complex: A missing link in the Proterozoic basement of the North Atlantic region. *Geology*, **20**, 1043-1046, https://doi.org/10.1130/0091-7613(1992)020<1043:rcamli>2.3.co;2.

Mulder, J.A., Halpin, J.A., Daczko, N.R., Orth, K., Meffre, S., Thompson, J.M. and Morrissey, L.J. 2019. A Multiproxy provenance approach to uncovering the assembly of East Gondwana in Antarctica. *Geology*, **47**, 645-649, https://doi.org/10.1130/G45952.1.
Murphy, J. 2019. Appinite suites and their genetic relationship with coeval voluminous granitoid batholiths. *International Geology Review*, **62**, 1-31, https://doi.org/10.1080/00206814.2019.1630859.
Murphy, J.B. 2013. Appinite suites: A record of the role of water in the genesis, transport, emplacement and crystallization of magma. *Earth-Science Reviews*, **119**, 35-59, https://doi.org/10.1016/j.earscirev.2013.02.002.
Nauton-Fourteu, M., Tyrrell, S., Morton, A., Mark, C., O'Sullivan, G.J. and Chew, D.M. 2020. Constraining recycled detritus in quartz-rich sandstones: Insights from a multi-proxy provenance study of the Mid-Carboniferous, Clare Basin, western Ireland. *Basin Research*, **33** 342-363, https://doi.org/10.1111/bre.12469.
Nutman, A.P. and Friend, C.R.L. 2007. Adjacent terranes with ca. 2715 and 2650Ma high-pressure metamorphic assemblages in the Nuuk region of the North Atlantic Craton, southern West Greenland: Complexities of Neoarchaean collisional orogeny. *Precambrian Research*, **155**, 159-203, https://doi.org/10.1016/j.precamres.2006.12.009.
O'Sullivan, G., Chew, D., Kenny, G., Henrichs, I. and Mulligan, D. 2020. The trace element composition of apatite and its application to detrital provenance studies. *Earth-Science Reviews*, **201**, 103044, https://doi.org/10.1016/j.earscirev.2019.103044.
O'Sullivan, G.J. and Chew, D.M. 2020. The clastic record of a Wilson Cycle: Evidence from detrital apatite petrochronology of the Grampian-Taconic fore-arc. *Earth and Planetary Science Letters*, **552**, 116588, https://doi.org/10.1016/j.epsl.2020.116588.
O'Sullivan, G.J., Chew, D.M. and Samson, S.D. 2016. Detecting magma-poor orogens in the detrital record. *Geology*, **44**, 871-874, https://doi.org/10.1130/G38245.1.
O'Sullivan, G.J., Chew, D.M., Morton, A.C., Mark, C. and Henrichs, I.A. 2018. An Integrated Apatite Geochronology and Geochemistry Tool for Sedimentary Provenance Analysis. *Geochemistry Geophysics Geosystems*, **19**, 1309-1326, https://doi.org/10.1002/2017gc007343.
Oswald, D.H. 1955. The Carboniferous Rocks between the Ox Mountains and Donegal Bay. *Quarterly Journal of the Geological Society*, **111**, 167-186, https://doi.org/10.1144/gsl.jgs.1955.111.01-04.09.
Owen, G. 2003. Load structures: Gravity-driven sediment mobilization in the shallow subsurface. *Geological Society, London, Special Publications*, **216**, 21-34, https://doi.org/10.1144/GSL.SP.2003.216.01.03.
Paton, C., Hellstrom, J., Paul, B., Woodheadb, J. and Hergt, J. 2011. Iolite: Freeware for the visualisation and processing of mass spectrometric data. *J. Anal. At. Spectrom.*, **26**, 2508-2518, https://doi.org/10.1039/C1JA10172B.
Petrus, J.A. and Kamber, B.S. 2012. VizualAge: A novel approach to laser ablation ICP-MS U-Pb geochronology data reduction. *Geostandards and Geoanalytical Research*, **36**, 247-270, https://doi.org/10.1111/j.1751-908X.2012.00158.x.
Pettijohn, F., Potter, P.E. and Siever, R. 1987. Introduction and source materials *Sand and sandstone*. Springer, 1-21, https://doi.org/10.1007/978-1-4612-1066-5_1.
Pettijohn, F.J., Potter, P.E. and Siever, R. 2012. Sand and Sandstone. Springer Science and business Media, New York, Berlin, 553.
Philcox, M., Baily, H., Clayton, G. and Sevastopulo, G. 1992. Evolution of the Carboniferous Lough Allen Basin, Northwest Ireland. *Geological Society, London, Special Publications*, **62**, 203-215, https://doi.org/10.1144/GSL.SP.1992.062.01.18.
Pointon, M.A., Cliff, R.A. and Chew, D.M. 2012. The provenance of Western Irish Namurian Basin sedimentary strata inferred using detrital zircon U–Pb LA-ICP-MS geochronology. *Geological Journal*, **47**, 77-98, https://doi.org/10.1002/gj.1335.

Pulham, A.J. 1989. Controls on internal structure and architecture of sandstone bodies within Upper Carboniferous fluvial-dominated deltas, County Clare, western Ireland. *Geological Society, London, Special Publications*, **41**, 179-203, https://doi.org/10.1144/gsl.sp.1989.041.01.14.
Rossi, C., Kälin, O., Arribas, J. and Tortosa, A. 2002. Diagenesis, provenance and reservoir quality of Triassic TAGI sandstones from Ourhoud field, Berkine (Ghadames) Basin, Algeria. *Marine and Petroleum Geology*, **19**, 117-142, https://doi.org/10.1016/S0264-8172(02)00004-1.
Scanlon, R., Daly, J.S. and Mj, W. 2003. The c. 1.8 Ga Stanton Banks Terrane, offshore Western Scotland, a large juvenile Palaeoproterozoic crustal block within the accretionary Lewisian complex. *Geophysical Research Abstracts*, **5**,
https://doi.org/https://ui.adsabs.harvard.edu/abs/2003EAEJA....13248S/abstract.
Schoene, B. and Bowring, S.A. 2006. U–Pb systematics of the McClure Mountain syenite: thermochronological constraints on the age of the 40Ar/39Ar standard MMhb. *Contributions to Mineralogy & Petrology*, https://doi.org/10.1007/s00410-006-0077-4.
Scotese, C.R. and McKerrow, W.S. 1990. Revised world maps and introduction. *Geological Society, London, Memoirs*, **12**, 1-21, https://doi.org/10.1144/GSL.MEM.1990.012.01.01.
Sevastopulo, G.D. and Wyse Jackson, P.N. 2009. Carboniferous: Mississippian (Tournaisian and Viséan). In The Geology of Ireland, Second Edition. *In*: Sanders, C.H.H.I.S. (ed.). Edinburgh: Dunedin Academic Press Ltd.
Sláma, J., Košler, J. *et al.* 2008. Plešovice zircon—a new natural reference material for U–Pb and Hf isotopic microanalysis. *Chemical Geology*, **249**, 1-35,
https://doi.org/10.1016/j.chemgeo.2007.11.005.
Somerville, I.D., Cózar, P., Aretz, M., Herbig, H.-G., Mitchell, W.I. and Medina-Varea, P. 2009. Carbonate facies and biostromal distribution in a tectonically controlled platform in northwest Ireland during the late Viséan (Mississippian). *Proceedings of the Yorkshire Geological Society*, **57**, 165-192, https://doi.org/10.1144/pygs.57.3-4.165.
Sorby, H. 1880. On the structure and origin of non-calcareous stratified rocks. *Quarterly Journal of the Geological Society of London*, **36**, 46-84.
Souders, A.K. and Sylvester, P.J. 2010. Accuracy and precision of non-matrix-matched calibration for lead isotope ratio measurements of lead-poor minerals by LA-MC-ICPMS. *Journal of Analytical Atomic Spectrometry*, **25**, 975-988.
Stacey, J.t. and Kramers, J. 1975. Approximation of terrestrial lead isotope evolution by a two-stage model. *Earth and Planetary Science Letters*, **26**, 207-221, https://doi.org/10.1016/0012-821X(75)90088-6.
Stephenson, D., Mendum, J.R., Fettes, D.J. and Leslie, A.G. 2013. The Dalradian rocks of Scotland: an introduction. *Proceedings of the Geologists' Association*, **124**, 3-82,
https://doi.org/10.1016/j.pgeola.2012.06.002.
Strachan, R.A., Alsop, G.I., Ramezani, J., Frazer, R.E., Burns, I.M. and Holdsworth, R.E. 2020. Patterns of Silurian deformation and magmatism during sinistral oblique convergence, northern Scottish Caledonides. *Journal of the Geological Society*, **177**, 893-910, https://doi.org/10.1144/jgs2020-039.
Thomson, S.N., Gehrels, G.E., Ruiz, J. and Buchwaldt, R. 2012. Routine low-damage apatite U-Pb dating using laser ablation–multicollector–ICPMS. *Geochemistry, Geophysics, Geosystems*, **13**,
https://doi.org/10.1029/2011GC003928.
Tinker, J., de Wit, M. and Brown, R. 2008. Linking source and sink: Evaluating the balance between onshore erosion and offshore sediment accumulation since Gondwana break-up, South Africa. *Tectonophysics*, **455**, 94-103, https://doi.org/10.1016/j.tecto.2007.11.040.
Tyrrell, S., Haughton, P.D.W. and Daly, J.S. 2007. Drainage reorganization during breakup of Pangea revealed by in-situ Pb isotopic analysis of detrital K-feldspar. *Geology*, **35**, 971-974,
https://doi.org/10.1130/g4123a.1.
Tyrrell, S., Haughton, P.D., Daly, J.S. and Shannon, P.M. 2012. The Pb isotopic composition of detrital K-feldspar: A tool for constraining provenance, sedimentary processes and paleodrainage.

Quantitative Mineralogy and Microanalysis of Sediments and Sedimentary Rocks. Mineralogical Association of Canada, Short Course Series, **42**, 203-217.
Tyrrell, S., Leleu, S., Souders, A.K., Haughton, P.D.W. and Daly, J.S. 2009. K-feldspar sand-grain provenance in the Triassic, west of Shetland: distinguishing first-cycle and recycled sediment sources? *Geological Journal*, **44**, 692-710, https://doi.org/10.1002/gj.1185.
Tyrrell, S., Souders, A.K., Haughton, P.D.W., Daly, J.S. and Shannon, P.M. 2010. Sedimentology, sandstone provenance and palaeodrainage on the eastern Rockall Basin margin: evidence from the Pb isotopic composition of detrital K-feldspar. *Geological Society, London, Petroleum Geology Conference series*, **7**, 937-952, https://doi.org/10.1144/0070937.
Vermeesch, P. 2004. How many grains are needed for a provenance study? *Earth and Planetary Science Letters*, **224**, 441-451, https://doi.org/10.1016/j.epsl.2004.05.037.
von Eynatten, H. and Dunkl, I. 2012. Assessing the sediment factory: The role of single grain analysis. *Earth-Science Reviews*, **115**, 97-120, https://doi.org/10.1016/j.earscirev.2012.08.001.
Whitehouse, M.J. and Moorbath, S. 1986. Pb–Pb systematics of Lewisian gneisses—implications for crustal differentiation. *Nature*, **319**, 488-489, https://doi.org/10.1038/319488a0.
Wiedenbeck, M., Alle, P. *et al.* 1995. Three natural zircon standards for U-Th-Pb, Lu-Hf, trace element and REE analyses. *Geostandards newsletter*, **19**, 1-23, https://doi.org/10.1111/j.1751-908X.1995.tb00147.x.
Woodcock, N.H. and Strachan, R.A. 2009. *Geological history of Britain and Ireland*. John Wiley & Sons.
Woodhead, J.D., Hellstrom, J., Hergt, J.M., Greig, A. and Maas, R. 2007. Isotopic and elemental imaging of geological materials by laser ablation inductively coupled plasma-mass spectrometry. *Geostandards and Geoanalytical Research*, **31**, 331-343, https://doi.org/10.1111/j.1751-908X.2007.00104.x.
Worthington, R.P. and Walsh, J.J. 2011. Structure of Lower Carboniferous basins of NW Ireland, and its implications for structural inheritance and Cenozoic faulting. *Journal of Structural Geology*, **33**, 1285-1299, https://doi.org/10.1016/j.jsg.2011.05.001.
Yan, Y., Xia, B., Lin, G., Cui, X., Hu, X., Yan, P. and Zhang, F. 2007. Geochemistry of the sedimentary rocks from the Nanxiong Basin, South China and implications for provenance, paleoenvironment and paleoclimate at the K/T boundary. *Sedimentary Geology*, **197**, 127-140, https://doi.org/10.1016/j.sedgeo.2006.09.004.

Figure Captions

Fig. 1: Geological map of NW Ireland. A, B & C are detailed in Figure 2. Bottom right: Map of Ireland outlining the position of North West Carboniferous Basin (NWCB).

Fig. 2: Detailed geological maps A: showing location Bunatrahir West (location 1) and Kilcummin (location 2) after (Graham, 1996; 2010); B: Carrowmoran (location 3); and C: Bundoran (location 4a) and Mullaghmore Head (location 4b) (adapted from GSI maps). Position of samples 1-4b are also shown.

Fig. 3: Schematic diagram illustrating the controls on sediment delivery to basins.

Fig. 4: Basic lithostratigraphic correlation of the MSFm at various locations with sample locations marked. Locations 1 & 2 are underlain by limestones; locations 3 & 4a/4b are underlain by shales. TNS: top not seen; BNS: base not seen.

Fig. 5: Location of Ireland and UK during the Carboniferous with potential source areas/topographic highs indicated. GB (Grampian Belt); GGF (Great Glen Fault); HBF (Highland Boundary Fault); ? represents the possible position of granites associated with GGF; for all other abbreviations see table 1.

Fig. 6: Selected thin section photomicrographs highlighting general petrography of the MSFm sandstones. Some representative grains have been outlined and labelled. Note sample 1 is most abundant in K-feldspar, while sample 4a is poorly sorted.

Fig. 7: $^{206}Pb/^{204}Pb$ versus $^{207}Pb/^{204}Pb$ plot of K-feldspars from all locations. Each source terrane defines a broad but largely unique Pb isotopic signature, represented by coloured polygons on the plots. Error bars are included on data points. The typical Pb growth curve is superimposed for reference.

Fig. 8: Detrital Zircon (dark grey) and apatite (red) Kernal Density Estimates (KDE) plots for each sample/location. These have been plotted with a bandwidth of 30Ma.

Fig. 9: RHS: Plots of log Sr/Y vs log LREE for detrital apatite. The points are coloured to show U-Pb age. Grey data points did not yield ages. Fields are defined through the application of a machine learning classifier (support vector machine) to a reference dataset of known compositions (O'Sullivan et al., 2020). LM = Low-medium grade metamorphic; HM = High grade metamorphic; I+M = Low ASI I type and mafic igneous; UM = Ultra mafic; S = S and I type granitoids. LHS: Summary pie charts showing the distribution of apatite source lithology type in each sample/location.

Fig. 10: a) KDE plots for each distinct basement terrane lithology (derived from trace elements in apatite) versus U-Pb age. All samples/locations are plotted to identify ages of source terrane type. LM = low grade metamorphic; HM = high grade metamorphic; I+M = I type granitoids and mafic igneous; UM = ultramafic; S = S type granitoids. Bandwidth is 30Ma. b) Histogram and probability density curves for Caledonian-aged grains only (350 Ma – 500 Ma), from all samples/locations, enabling more precise illustration/identification of Caledonian age peaks. Bin size is 10 Ma.

Fig. 11: Schematic palaeodrainage block diagram showing sourcelands feeding the various sample/location positions within the basin Scale is exaggerated from hinterland to basinal area. KET

(Ketilidian Belt); NAC (North Atlantic Craton); NAQ (Nagssugtoqidian); RB (Rockall Bank); LEW (Lewisian); PB (Porcupine Bank); SB (Stanton Banks); RC (Rhinn's Complex); AGC (Annagh Gneiss Complex); DS (Dalradian Supergroup); BTW (Bunatrahir West); KC (Kilcummin); CWM (Carrowmoran); BD (Bundoran); MH (Mullaghmore Head).

Fig. 12: Detrital zircon U-Pb age ranges from the Dalradian Supergroup (after Cawood et al., 2003) compared with detrital zircon U-Pb from the sample/locations of MSFm. Dark yellow bands represent the significant zircon peaks, with lighter yellow representing minor peaks.

Table 1: Source terranes summarised with U-Pb ages and Pb isotopic ratios.

Table 2: Sample locations, locality names and sample names, including depositional system setting, at each location.

Table 3: Summary table of the interpreted detrital grain populations and their correlative source terranes.

Figure 1

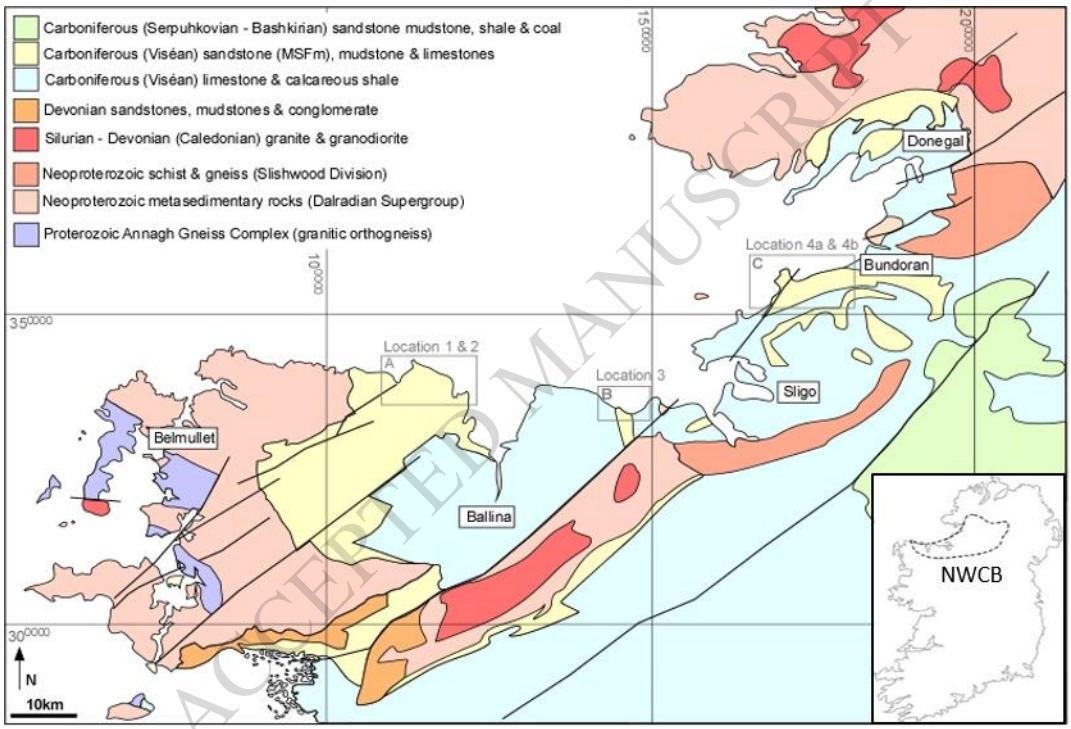

Figure 2

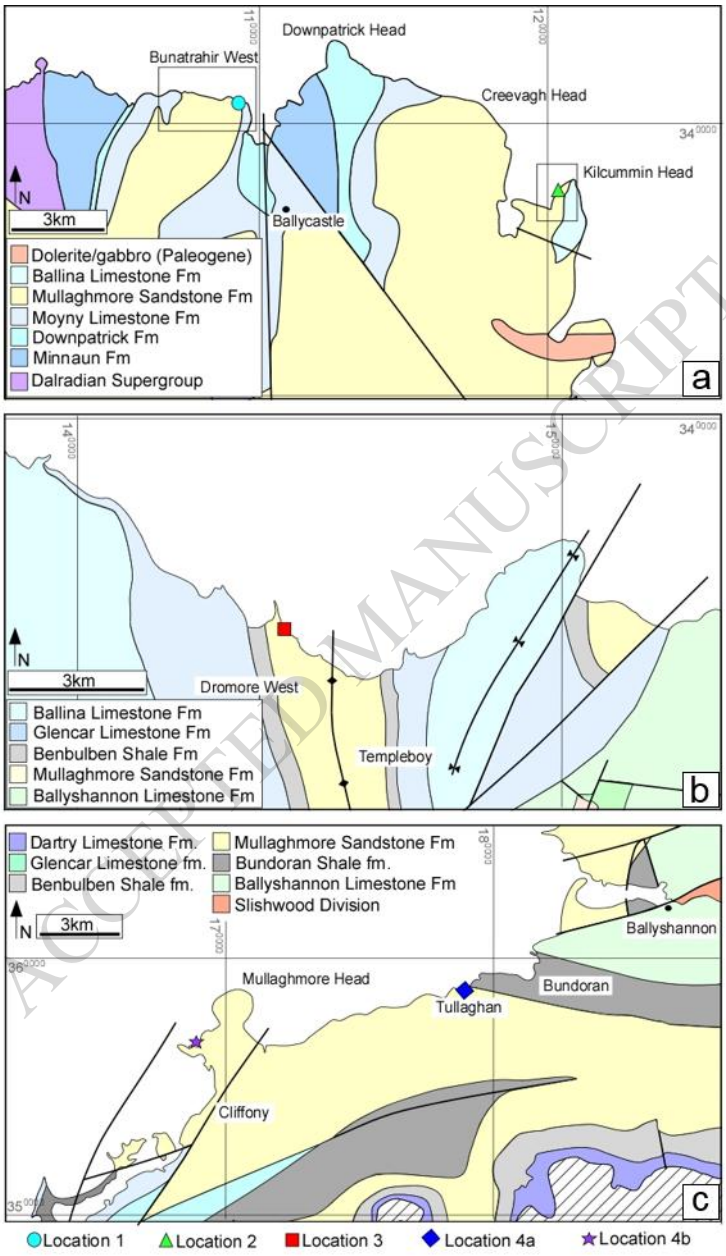

Figure 3

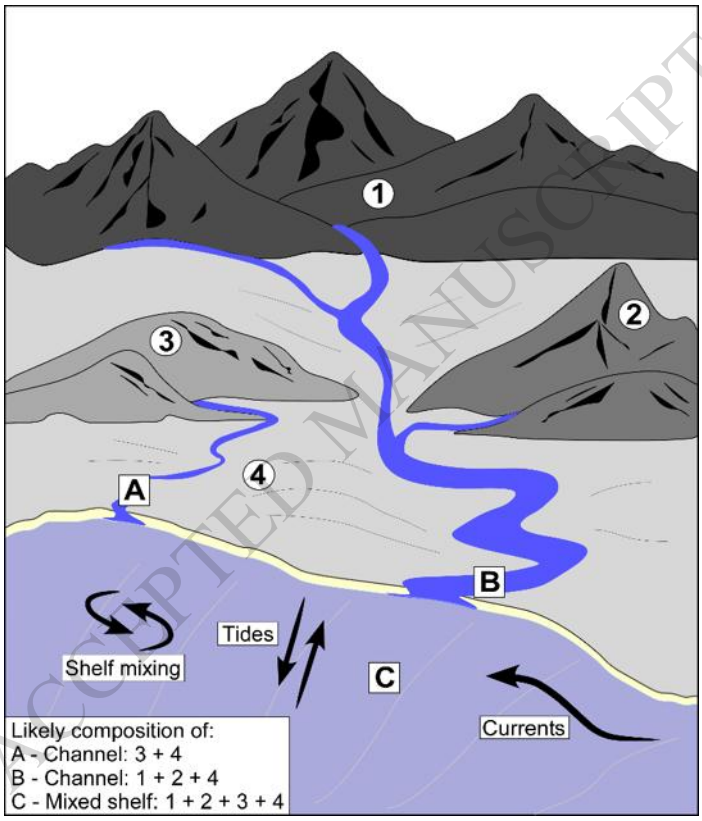

Figure 4

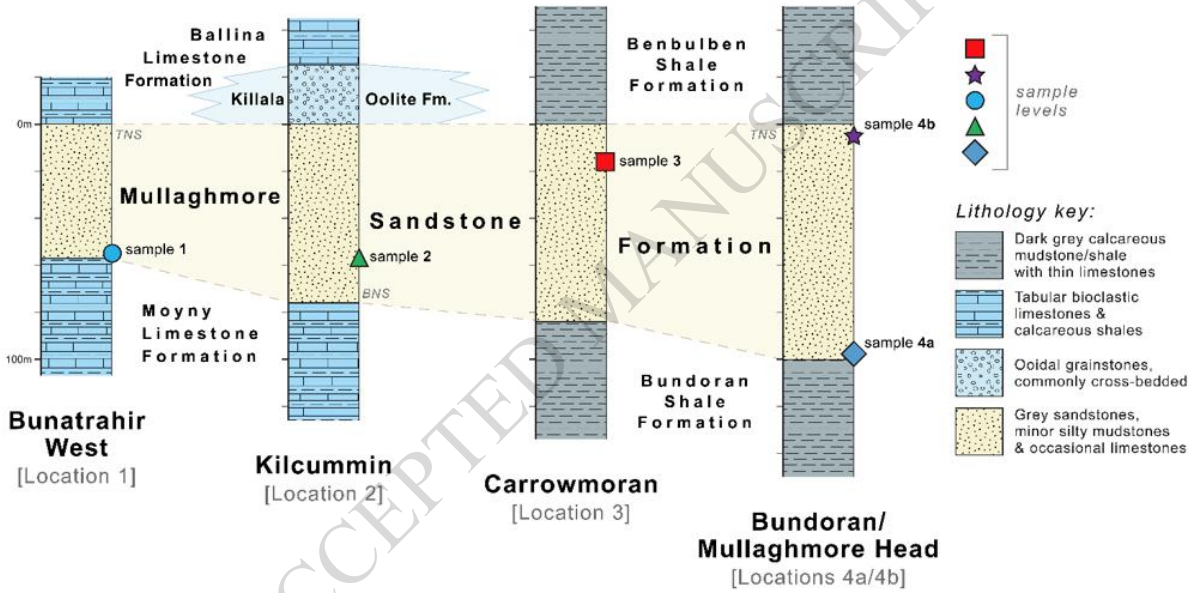

Figure 5

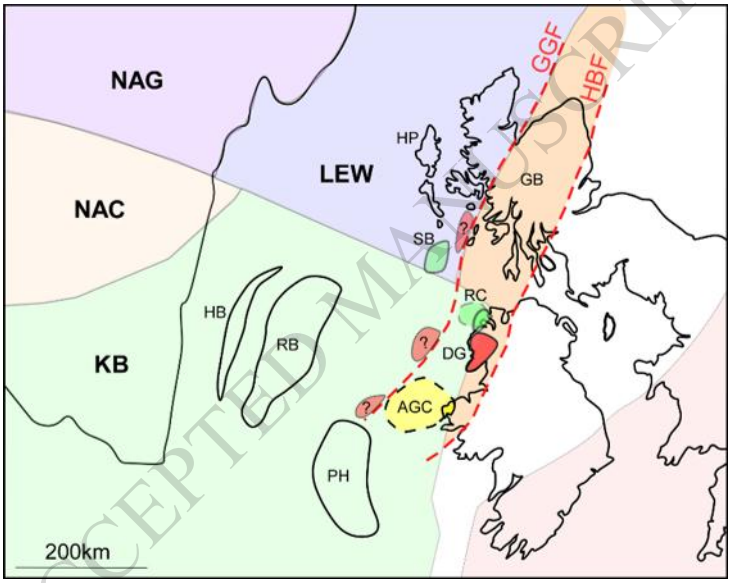

Figure 6

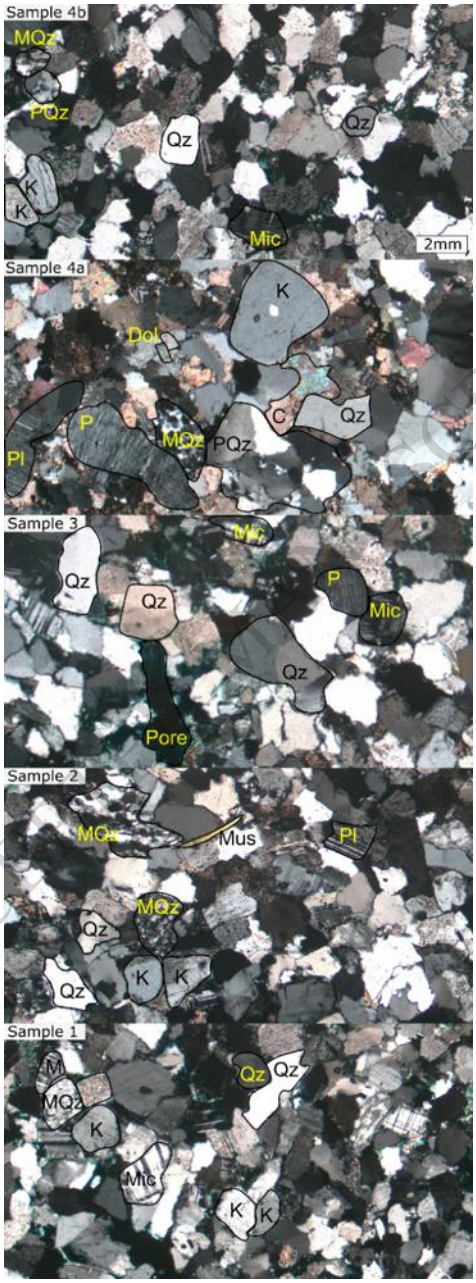

Figure 7

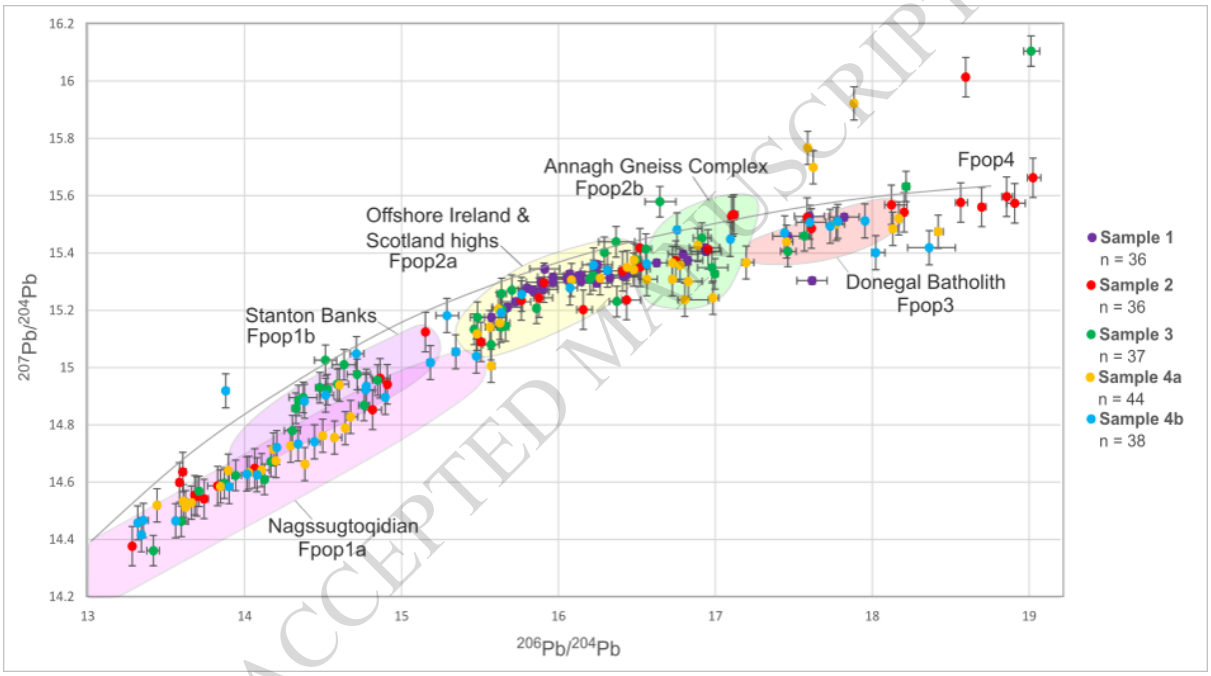

Figure 8

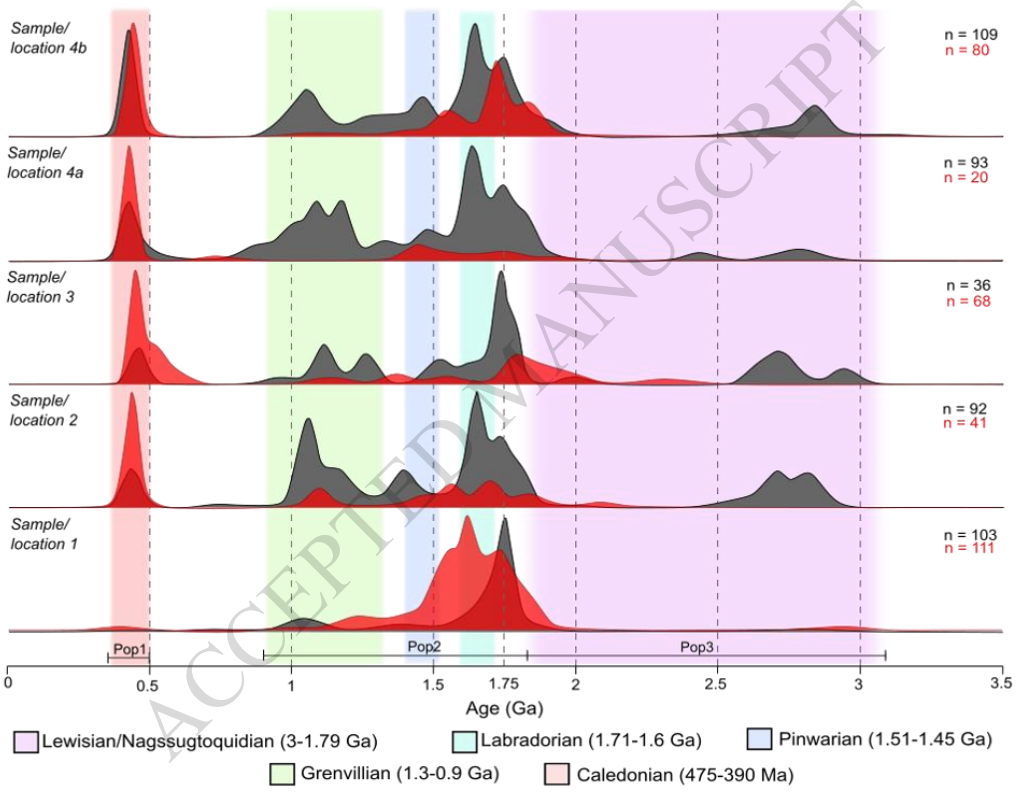

Figure 9

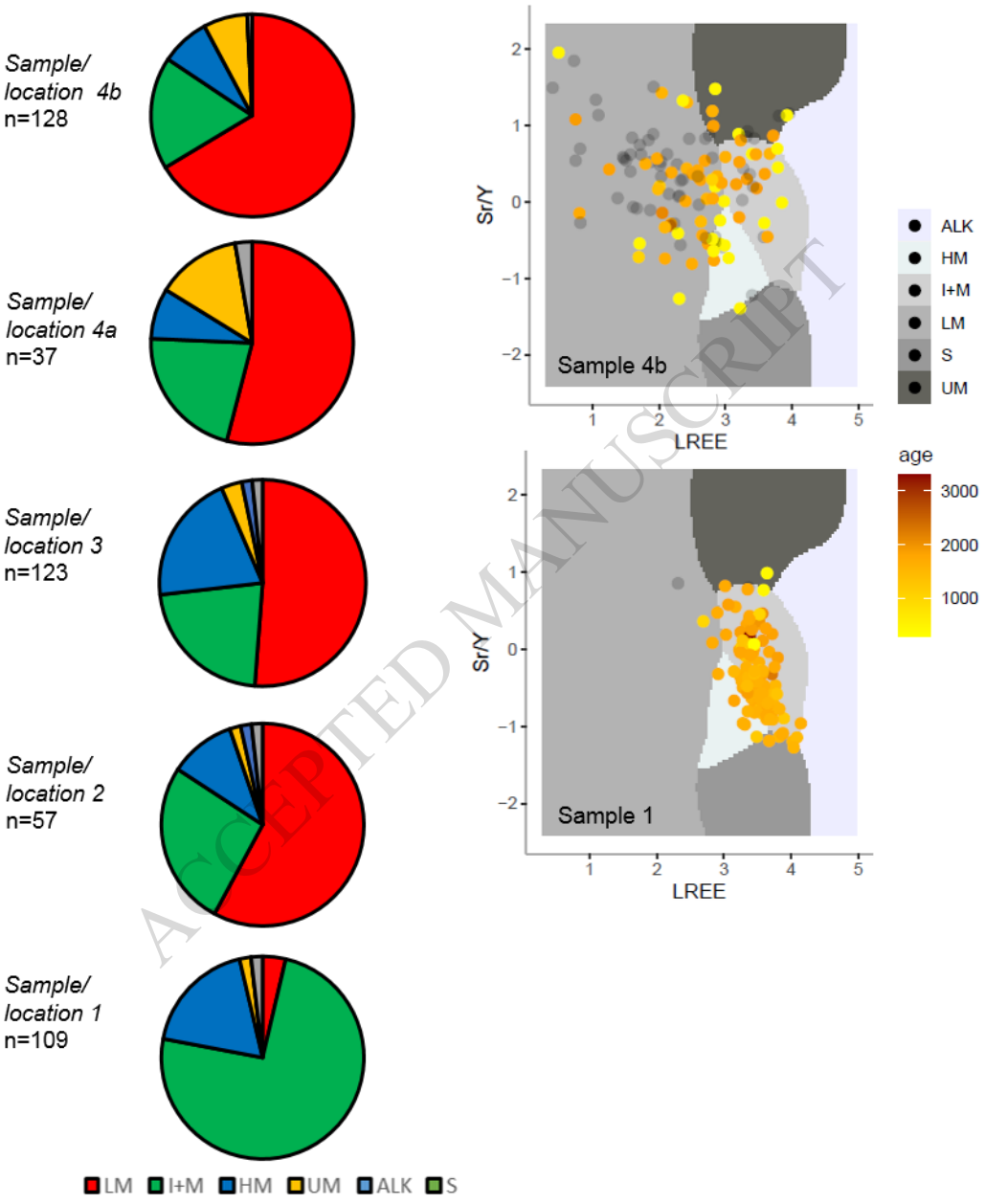

Figure 10

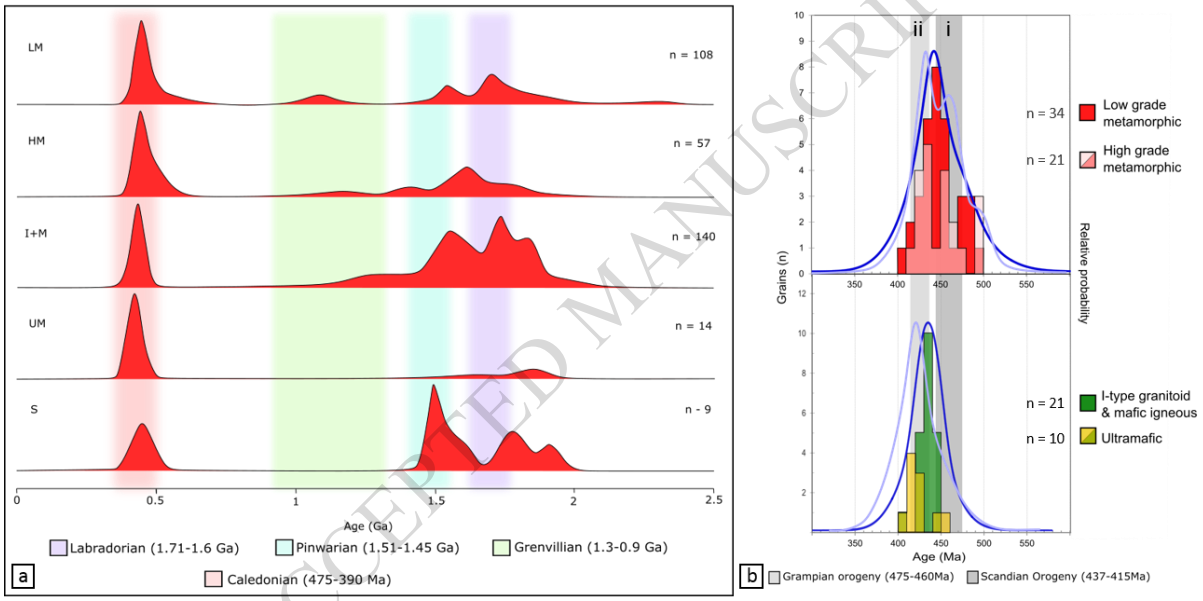

Figure 11

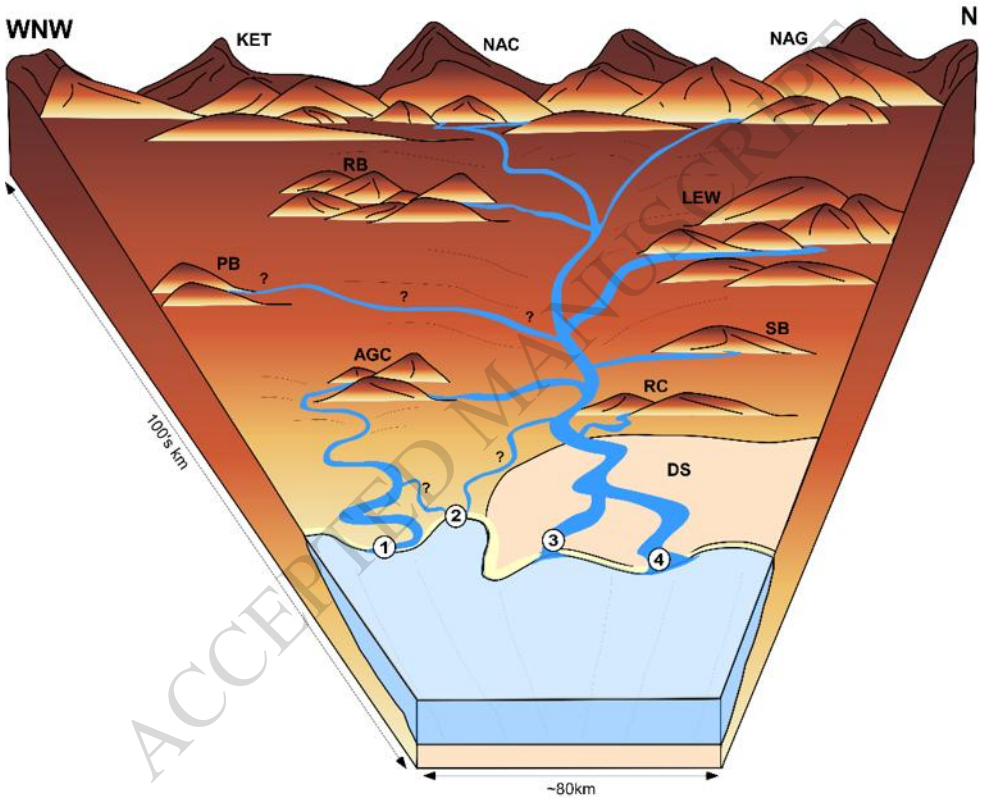

Figure 12

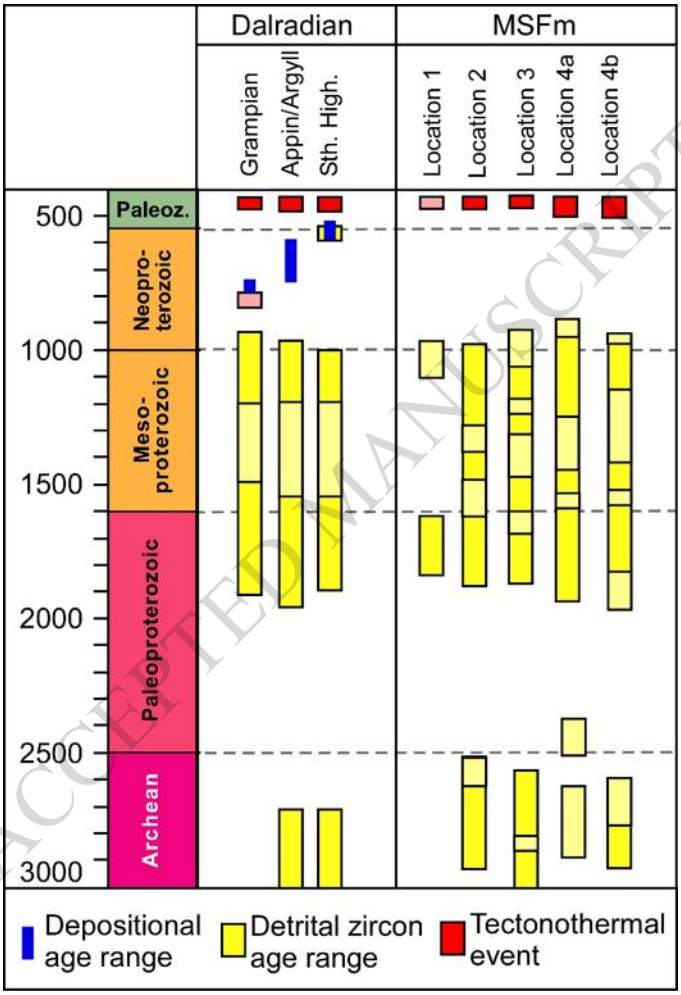

Terrane/crustal affinity	*Location*	*Zircon U-Pb Age range*	*K-feldspar $^{206}Pb/^{204}Pb$*
NAG (Nagssugtoqidian)	*S.E. Greenland*	*>1.95 – 1.8 Ga*	*13 - 15.5*
NAC (North Atlantic Craton)	*S. Greenland*	*>2.5 Ga*	
KB (Ketilidian Belt)	*S. Greenland*	*1.85 – 1.72 Ga*	
LEW (Lewisian Complex)	*Stanton Banks*	*>1.83 – 1.79 Ga*	*13.9 - 15.3*
'Laurentian affinity' (offshore Ireland/Scotland highs)	*RC (Rhinns Complex), RB (Rockall Bank), HB (Hatton Bank), PH (Porcupine High)*	*1.79 – 1.3 Ga*	*15.5 - 16.5*
AGC (Annagh Gneiss Complex)	*Annagh Gneiss Complex*	*1.75 Ga & 1.3 – 0.96 Ga*	*16.5 - 17.3*
DS (Dalradian Supergroup)	*NW Ireland, NW Scotland*	*3.2 – 0.5 Ga*	
Caledonian Orogenic association	*NW Ireland/Scotland e.g. Donegal Granite*	*475 - 390 Ma*	*>17.3*

Table 1:

Locations	Location	Grid reference	Sample name	Type channel	System setting
Location 1	Bunatrahir West	109357, 340907	Sample 1	Basal	Most proximal/fluvial
Location 2	Kilcummin	120320, 337950	Sample 2	Representative near base	Interdistributary bay
Location 3	Carrowmoran	144336, 335401	Sample 3	Representative near top channel	Lateral delta lobe
Location 4a	Bundoran	180277, 358978	Sample 4a	Basal	Proximal
Location 4b	Mullaghmore Head	169276, 356380	Sample 4b	A topmost channel	Proximal

Table 2:

Feldspar	*Zircon*	*Apatite*	*Terrane/crustal affinity*	*Location*	*Age range*	*$^{206}Pb/^{204}Pb$*
Fpop1a	*Zpop1*	*Apop1*	*NAG (Nagssugtoqidian)*	*SE Greenland*	*>1.95 – 1.8 Ga*	*13 - 15.5*
Fpop1b			*LEW (Lewisian Complex)*	*Stanton Banks*	*>1.83 – 1.79 Ga*	*13.9 - 15.3*
Fpop2a	*Zpop2*	*Apop2*	*'Laurentian affinity' (offshore Ireland/Scotland highs)*	*RB (Rockall Bank), RC (Rhinns Complex), PH (Porcupine High)*	*1.79 – 1.3 Ga*	*15.5 - 16.5*
Fpop2b			*AGC (Annagh Gneiss Complex)*	*Annagh Gneiss Complex*	*1.75 Ga & 1.3 – 0.96 Ga*	*16.5 - 17.3*
Fpop3	*Zpop3*	*Apop3*	*Caledonian Orogenic association (including Dalradian Supergroup)*	*NW Ireland/Scotland e.g. Donegal Granite*	*475 - 390 Ma*	*>17.3*

Table 3: